Delft University of Technology

Developement of the Experimental Design for the Validation of EEG Source Localization With fMRI

Application of a Haptic Robot to Identify Active Neuronal Ensembles

T.J. van Rooijen
Study number: 4133994

Examination Committee:
F.C.T. van der Helm; BioMechanical Engineering, TU Delft (chair)
K. Rassels; BioMechanical Engineering, TU Delft
P.J. French; Bioelectronics, TU Delft

Development of the Experimental Design for the Validation of EEG Source Localization With fMRI

Application of a Haptic Robot to Identify Active Neuronal Ensembles

Abstract

Various source localization algorithms exist to perform localization with High Density (HD)-ElectroEncephaloGraphy (EEG). However, validation of these EEG source localization algorithms is lacking. The current gold standard for source localization in the brain is functional Magnetic Resonance Imaging (fMRI) by calculating the difference in hemodynamic response to different stimuli. This study aims to validate HD-EEG source localization with fMRI using an MR compatible haptic robot. Participants performed several tasks with the robot to activate cortex patches and allow localization of source activity under various circumstances. These hypothesized patches are the somatosensory, motor and visual cortex. No comparison is made with fMRI due to time constraints. As no comparison could be made, we aim to validate the experimental methodology. Activation of the somatosensory cortex is clearly visible. The visual cortex is often localized, but lacks power in some settings. Activity during the torque task can be localized, but not conclusively to the motor cortex. In all, the experiment was a success, as it was able to induce verifiable different brain states. Hypothesized task contrasts contained different activity distributions. Improvements can be made by generating a more detailed leadfield and by applying a linear manipulator.

Acknowledgement

I want to thank my supervisors Frans van der Helm, Kianoush Rassels, Joris van der Cruijssen and Fleur van Rooteslaar for their patience and guidance and the learning opportunities created for me during the fulfillment of this thesis project.

Acronyms

APs Action Potentials. 11

BEM Boundary-Element-Method. 12, 24

BOLD Blood-Oxygen-Level-Dependent. 3, 9

CNS Central Nervous System. 7, 8, 31

dHb Deoxyhemoglobin. 3

DICS Dynamic Imaging of Coherent Sources. 12, 15, 16, 23

dSPM dynamic Statistical Parametric Mapping. 4, 12

DTI Diffusion Tensor Imaging. 11, 24

EEG ElectroEncephaloGraphy. 1, 3–5, 7–12, 24, 30, 31

EMG ElectroMyoGraphy. 4, 5, 7, 9, 10, 30, 31

ERP Event-Related Potential. 10, 12–19, 23–25

FEM Finite-Element-Method. 24

fMRI functional Magnetic Resonance Imaging. 1, 3–5, 8, 9, 11, 25

Hb OxyHemoglobin. 3

HD High Density. 1, 3

ICA Independent Component Analysis. 13, 25

MNE Minimum Norm Estimation. 3, 12, 15

MR PoPe MR Compatible Wrist Manipulator (MR Pols Perturbator). 4–10, 12, 24, 25, 30, 31

MRI Magnetic Resonance Imaging. 4, 5, 11, 12, 14–16, 24

MVC Maximum Voluntary Contraction. 7, 10

SL Source Localization. 4, 5, 8, 10–12, 14–21, 23–25

SNR Signal to Noise Ratio. 12

TF Time-Frequency. 15–17, 19, 22, 23, 25

TFR Time-Frequency Response. 14, 16–21, 23–25

Contents

1 Introduction

The brain has been a topic of interest ever since we had a basic understanding of the human body. It processes the information received from our senses, memorizes our past experiences, and dictates what we do and how we behave. In short, it regulates how we interact with the world around us. Unfortunately, there are also many neurological diseases that can impair these functions, such as ischemic stroke [6], Parkinson's disease [12], and migraines [47]. If we want to understand how these neurological diseases affect the brain, we need to gain insight into the brain's normal function. Various measuring modalities allow us to gain this insight in normal and diseased functioning of the brain. Two of the primary, non-invasive brain functional recording devices are High Density (HD)-ElectroEncephaloGraphy (EEG) and functional Magnetic Resonance Imaging (fMRI).

HD-EEG directly measures the electric potentials generated by neuronal ensembles in the cortex by placing electrodes on the scalp [14]. HD-EEG can acquire the data at a high sampling frequency [4]. It is cheap and mobile. The output of the EEG is the voltage, which is measured per electrode compared to the common average. These voltage measurements do not represent the activity of the brain, as these are signals are a mixture of dipoless originating from highly localized locations [31]. Pyramidal cells are present throughout the gray matter, creating dipole moments when activated or inhibited. When these ensembles are arranged correctly and activate or inhibit synchronous, they can generate a dipole moment large enough to be detected by the EEG electrodes. This dipole signal can be found in every electrode with a favorable orientation and location. As such, electrodes "see" all kinds of dipoles located throughout the grey matter and the voltage measurement represents a mixed signal.

The EEG recordings can be used to locate sources in the brain. When the distribution of tissues in the head is known, as well as the placement of electrodes and the location of the cortical areas where EEG sources are present, the activity of these cortical areas can be calculated by inversing the calculation from source to electrode. However, the true spatial distribution of HD-EEG sources is not well defined [27], because the solution is unobservable. The amount of neurons in the brain is far larger than the amount of electrodes on the scalp during EEG. Hence, infinite source distributions can explain the EEG data.

To find a unique solution to the inverse problem, EEG source localization algorithms regulate the source localization with constraints. The inverse problem becomes an optimization problem within these constraints, which has seen many solutions over the years. The first solution is the Minimum Norm Estimation (MNE) [18], after which came many more, such as LORETA [39], DICS [16], and others. MNE finds the set of dipole vectors with the least squares solution explaining the measured data, which corresponds to Thikonov regularization. LORETA constraints the solution, such that the solution has maximum smoothness. LORETA can find deeper sources in the brain, while MNE primarily finds sources at the surface of the cortex. DICS localizes oscillatory power by averaging the power over a frequency band and calculating the cross-spectral-density accompanying the averaged frequency band. Then, a linear transformation matrix is applied, which is the inverse of the leadfield matrix and minimized by constraints, to estimate the cross-spectrum between source combinations. The power at a source node can be extracted from the cross spectral density between sources, as the auto-spectral density is contained within.

fMRI uses the metabolism of neurons to find the active cortical patches of the brain [29]. As neurons are activated/inhibited, they consume more oxygen. A change in metabolism induces a change in Deoxyhemoglobin (dHb) in the blood vessels. fMRI is an indirect measure of neuronal activity, because it measures the dHb concentration instead of electric potentials and is called the Blood-Oxygen-Level-Dependent (BOLD) signal. The localization is represented with voxels. An increase of dHb results in an attenuated BOLD signal. By contrasting two measurements, a change in the voxel output can be recognized, and thus, a change in dHb concentration. Hence, this change shows where source activity changes between tasks. fMRI has an excellent spatial resolution. It can produce images with voxels with submillimeter dimensions [30]. This reflects the accuracy of fMRI because a source is present somewhere close to that voxel. However, the temporal resolution of fMRI is poor, due to the slow hemodynamic response. The slow increase of blood flow to the active patch, as a reaction to neurons increased metabolic rate, reaches its peak 5-6 seconds after the neuronal activity has started.

Validation of HD-EEG is only possible if compared to a golden standard, such as fMRI. The measurements of these modalities are connected by the metabolism of the neuron. If the neuron is either excited or inhibited, it will consume more oxygen, which causes dilation of the veins in that area. The dilation causes more OxyHemoglobin (Hb) to rush to the site and the dHb concentration to decrease, increasing the BOLD signal [20, 7].

The possibility still exists for EEG and fMRI to point to slightly different locations. EEG measures the activity of neurons in the brain, generated by dendrites of neurons. fMRI cannot easily differentiate between top-down and bottom-up signals, excitation, inhibition, task-specific processes and neuromodulation [28]. Furthermore, EEG measures the fast electrical activity of dipoles, allowing insight into fast dynamics. fMRI measures the slow hemodynamic system, which filters out these fast dynamics.

1.1 Problem Statement

Multiple algorithms exist that can perform source localization with EEG data. Each algorithm has its strengths and weaknesses. Such localization algorithms are often only validated by themselves when compared to a gold standard [2, 13, 22, 21, 23, 24, 25, 35, 42, 50, 51, 53, 55]. The validation is also done using simulated data only [54]. The problem is that comparisons of multiple EEG source localization algorithms compared to a golden standard, such as fMRI, are lacking. Two studies compared multiple source localization algorithms to a gold standard with real data [5, 46]. Inter study comparison of results is also difficult due to different data processing and outcome variables (Euclidean Distance [13] vs Pearson's Rho [19]) and different experimental setups, such as a different number of electrodes [23, 48]. No optimal algorithm can be found, as the numerous confounding factors differ between studies. The algorithm closest to fMRI sources was found to be dynamic Statistical Parametric Mapping (dSPM) ([21]), but another study reported larger errors ([44]).

1.2 Study Aim

EEG source localization needs to be validated with a gold standard, such as fMRI. The aim of this study is to develop an experimental design capable of validating EEG SL algorithms.

1.3 Experimental Approach

The experimental protocol will be tested by activating the somatosensory, motor and visual cortex in various combinations. These different brain states are induced by performing different tasks with MR Compatible Wrist Manipulator (MR Pols Perturbator) (MR PoPe). This robot is able to convey a perturbation to the wrist of the participant, so that movements can easily be time locked. This robot is MRI compatible and can be applied in both the EEG and fMRI experimental setups. By enabling and disabling the perturbation, applying force to the robot, and giving visual feedback, different brain states are achieved. The following states are hypothesized:

- Applying a perturbation on the wrist by MR PoPe should activate the somatosensory cortex.
- Applying a constant force by the participant to the robot should activate the motor cortex.
- Receiving feedback from a screen on task performance will activate the visual cortex.

The task descriptions will include various combinations of the 3 hypotheses above. By inducing different brain states, the algorithm can be validated under various circumstances (single source, multiple sources, either close by or far apart).

The article will first explain the methods used for the experiments and source localization in detail. This includes the design of the various tasks, the design of the perturbation, the data acquisition, the signal processing of the robot and finally, the data processing of EEG and the source localization. Hereafter, the results of source localization for EEG are shown in the results section. Their locations compared to literature will be discussed, and conclusions will be drawn.

The comparison between fMRI and EEG will not be made in this article due to time constraints during the development of the experimental protocol. Source localization will only be performed on EEG data.

2 Materials and Methods

2.1 Medical Ethics Committee (MEC) Permission and Approval

The Medical Ethics Committee of the University Medical Centre Amsterdam approved the experimental protocol, the hardware system and the CE-marking before starting the research. The study was registered at the Dutch Trial Register (NTR) on July 30, 2020 with identification number NL8783. Thus, the experiment with human subjects for the research purpose are agreed upon.

2.2 Participants Experiment

Two healthy participants (ages 25 (number 001) and 33 (numbers 002 and 022), one female (001)) participated in this study as part of a pilot study towards the final protocol. One test subject was measured twice to measure reproducibility of the meaurements. Participants had to be 18 years old or older and be capable of working with MR PoPe. The exclusion criteria for this study were: (1) MR contra-indicators, (2) medication use that might influence brain activity, (3) neurological, psychiatric, or other disorders that might influence brain activity, (4) abnormalities in the hand/wrist or prior surgery in the hand/wrist, and (5) a history of alcohol or drug abuse. Both test subjects complied with the in- and exclusion criteria. All participants gave written informed consent.

The handedness of each participant was determined using the Edinburgh Handedness Inventory [36].The participant handednesses were right-handed and ambidextrous. Due to constraints in the design of MR PoPe (explained in Section 2.3.1) only the right hand can be used during the experiment.

2.3 Experimental Setup

The experimental setup consisted of an MR PoPe, an electroencephalogram EEG, a Magnetic Resonance Imaging (MRI) scanner, and ElectroMyoGraphy (EMG). The experiment included EEG measurements and an MRI head scan if possible. Participant

001 had no MRI taken due to time constraints. Preparations were made for the fMRI experiments. The EEG experimental setup of can be found in Appendix A.

2.3.1 The MR Compatible Wrist Manipulator

An MR-compatible wrist manipulator called MR PoPe [3] was used during the experiments. MR PoPe conveys a designed mechanical perturbation to the participant's wrist. The kind of perturbation conveyed to the participant is explained in Section 2.4.2. MR PoPe consists of two parts: an MR-compatible manipulandum and an MR-incompatible part. Figure 1 shows both parts of the robot. The compatible manipulandum must be inside the MRI scanner, while the incompatible part must stay outside the MRI room. MR PoPe was applied in a earlier experimental fMRI study [45].

The MR-compatible part (Figure 1a) was held by the participant while performing the experiment in the MRI machine. The white parts are in contact with the participant (arm rest and hand grip). The hand grip is connected to a hydraulic rotary vane motor. Sensors in the manipulandum allowed for the recording of force and position data of the hand grip. Nine meter long plastic tubing and fiber optic cables were used to convey oil and data between the MR-compatible and the MR-incompatible part. The MR-compatible part can be fastened to a table using glue clamps during the EEG experiment. It can be fastened in the table of the MRI machine when used during fMRI scanning.

The MR incompatible part, located outside of the MR room (fig. 1b) consists of the following:

- A real-time computer
- A servo drive
- An electric motor
- A hydraulic reversible gear pump
- An oil reservoir
- An attachment for two 9-meter-long oil tubes to the MR incompatible part
- Ports for the fiber optic cables

The servo drive processes the input from the computer and transforms it into a usable signal for the electromotor, which drives a hydraulic pump. As such, the velocity signal introduced to the computer is converted to an electrical signal for the electromotor, which is transformed into radial movement pressurizing the oil. The pressurization of oil moves the vane motor. The incompatible part obtains the force and position measurements from the MR-compatible part. It can send triggers to an amplifier to identify which task is being performed, to specify when a task has started and which motion type is being introduced to the participant. The MR incompatible part is not compatible with the MRI scanner, because ferromagnetic metal parts are present within. As such, it must be kept outside of the MRI room at all times. The long oil tubes and fiber optic cables circumvent this problem.

During EEG acquisition, the participant was seated relaxed and comfortably next to the manipulandum. The arm was positioned next to the body, and the elbow was under an 90° angle approximately. The right forearm was constrained in an arm brace, such that only the wrist could move. Only the right arm could be attached to the manipulandum, due to limitations in the arm brace positioning. As such, left-handed participants were only able to use their off-hand. The forearm was constrained so that the wrist rotation axis was above the rotation axis of the vane motor. The hand grip's position can be modulated so that the participant can comfortably grip the handle.

2.3.2 EEG Data Acquisition

EEG was acquired using a 128-electrode WaveGuard EEG cap (5/10 system, Al/AgCl electrodes, ANT Neuro, Netherlands) in combination with a 136-channel ReFa amplifier (TMSi, Netherlands). The ground electrode was placed on the right mastoid. The electrode distribution over each participant's head was measured with the Xensor system (ANT Neuro, Netherlands).

2.3.3 EMG Data Acquisition

EMG was acquired for the EMG feedback tasks. EMG was acquired during EEG with BlueSensor N electrodes (Ambu, Denmark). The measured muscles are the *m. flexor carpi radialis* and the *m. extensor carpi radialis brevis*.

Figure 2 shows the processing of the position perturbation and target force/EMG by the participant to the output data, where EEG measures brain activity, EMG measures muscle activity, and MR PoPe provides force and position measurements.

2.4 Experimental Protocol

The participants had to perform different tasks to put the brain in different brain states. Each brain state is associated with a different source distribution. These different source distributions allowed the Source Localization (SL) algorithms to be evaluated under different conditions. These conditions can include single sources, multiple sources, sources close to each other, and sources far apart. The aim is to activate the primary sensory, the primary motor, and the primary visual cortex in various combinations.

2.4.1 Task Design

Different brain states were induced by performing various tasks with MR PoPe. These different tasks adhere to a factorial design. These tasks were:

(a) The MR-compatible part of MR PoPe.

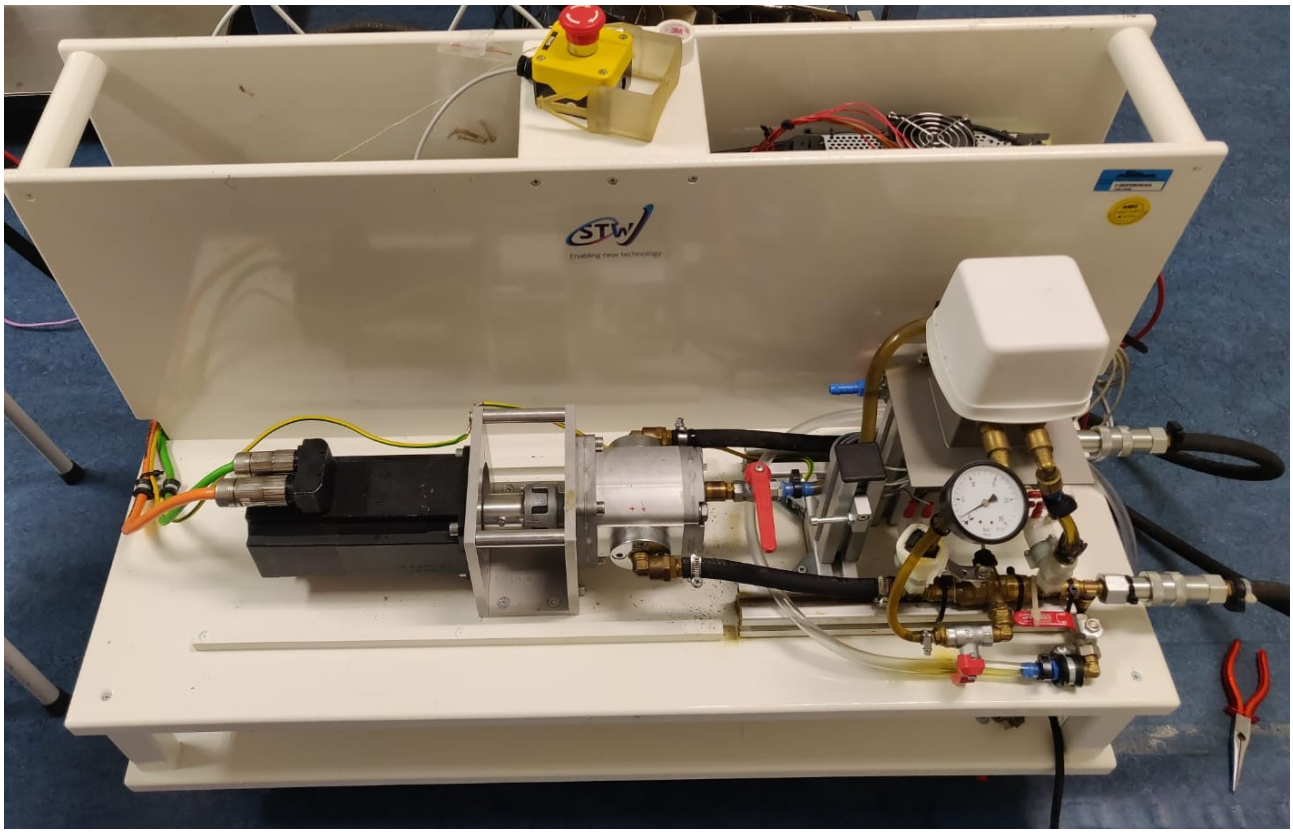

(b) The MR-incompatible part of MR PoPe.

Figure 1: Photos of the MR-compatible (1a) and MR-incompatible (1b) parts of MR PoPe. Figure 1a: The manipulandum is entirely made of plastics, as are the oil tubes and the glass fiber mantle. The participant's right forearm is constrained in an arm brace (left), while the wrist grasps the white hand grip. Figure 1b: At the front, the electromotor can be seen (the black block), the hydraulic pump connected to the electric motor, and the oil reservoir (under the white cap). The complex tubing system after the hydraulic pump is used to build up pressure inside the black tubing. In the gap between wooden panels are the real-time computer and the servo drive.

1. Rest task (no perturbation, no visual feedback, no active motor task).

2. Rest task with visual feedback

3. Relax task (perturbation present, no visual feedback present, no active motor task).

4. Relax task with visual feedback.

5. Constant torque task (20% of Maximum Voluntary Contraction (MVC), perturbation present, no visual feedback).

6. Constant torque task with visual feedback.

7. EMG task. Constant cocontraction of the forearm is expected from the participant (20% of maximum EMG output).

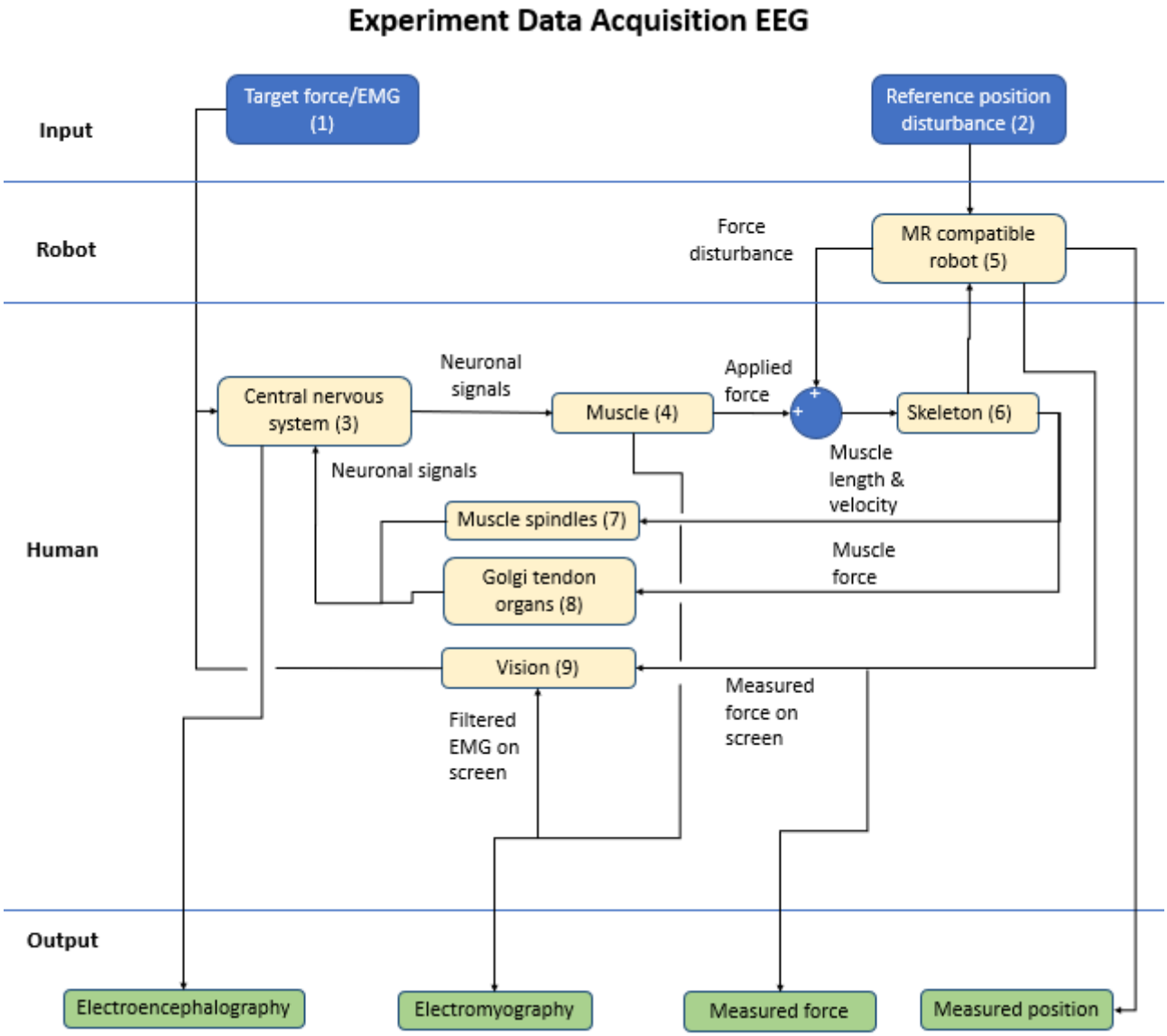

Figure 2: A block overview of the processed signals during the experiment. The input (target force/EMG (1)) is the force or EMG target the participant needs to achieve. The reference force is an internal value for the participant and shown by the screen. It is handled by the Central Nervous System (CNS) (3), which will relay a signal to the muscles (4) about what force to apply to the manipulandum and impedance to set in the wrist joint. The reference position disturbance (2) is the position profile the manipulandum needs to follow. MR PoPe (5) measures the displacement that needs to be created and applies a force to the manipulandum to move. The robot and the muscle force move the manipulandum and the skeleton (6) in a specific direction. The movement and force are picked up by muscle spindles (7) and Golgi tendon organs (8), while the actual applied force or filtered EMG, measured by the manipulandum or surface EMG electrodes, respectively, is seen on a screen (vision (9)). These signals are fed back to the CNS (3) to determine the following neuronal input. EEG data was collected from the CNS (brain), while EMG data was collected from the wrist muscles. MR PoPe (5) acquired data about the manipulandum position and force applied.

These tasks differ depending on various forms of inputs and participant induced outputs. The inputs are wrist perturbations generated by MR PoPe and visual feedback generated on a screen for both EEG and fMRI. The participant induced output is motor control (either applied torque or muscle activation). The sensory cortex should process the wrist perturbation, the visual cortex should process the visual feedback on task performance or visual perturbations, and the motor cortex should process the application of a constant torque to the manipulandum, constant muscle activation of the right forearm and responds to wrist perturbations.

fMRI can only identify sources by creating a contrast between different task designs. Therefor, a similar design is made for EEG SL. These trials can be contrasted, such that only certain functional brain areas are shown as activated.

No significance testing and SL will be performed on contrasts where both tasks activate different cortex patches, such as the Relax task without visual feedback and the Rest task with visual feedback. The previous only activates the somatosensory cortex, while the latter only activates the visual cortex.

As such, the activation of various combinations of cortex patches is hypothesized with the following contrasts:

- Somatosensory cortex only
    1. Relax task without visual feedback and Rest task without visual feedback (**1 vs 3**)
    2. Relax task with visual feedback and Rest task with visual feedback (**2 vs 4**)
- Visual cortex only
    1. Rest task with visual feedback and Rest task without visual feedback (**1 vs 2**)
    2. Relax task with visual feedback and Relax task without visual feedback (**3 vs 4**)
    3. Torque task with visual feedback and torque without visual feedback (**5 vs 6**)
- Motor cortex only
    1. Torque task without visual feedback and Relax task without visual feedback (**3 vs 5**)
    2. Torque task with visual feedback and Relax task with visual feedback (**4 vs 6**)
- Somatosensory and visual cortex
    1. Relax task with visual feedback and Rest task without visual feedback (**1 vs 4**)
- Somatosensory and motor cortex
    1. Torque task without visual feedback and Rest task without visual feedback (**1 vs 5**)
    2. Torque task with visual feedback and Rest task with visual feedback (**2 vs 6**)

Table 1: An overview of the activated cortex patches per task combination contrast. Each task induced a different brain state. EEG could identify the sources for each individual task. However, fMRI uses contrasts to determine the activated cortices. Hence, EEG should do the same when the localization of both modalities are compared. A + indicates the cortex patch is expected to be activated when contrasting the two tasks. A - indicates it the cortex patch is not hypothesized to be active.

	Activated cortex patches		
Compared tasks	Somatosensory	Visual	Motor
1 & 2	-	+	-
1 & 3	+	-	-
1 & 4	+	+	-
1 & 5	+	-	+
1 & 6	+	+	+
1 & 7	+	+	+
2 & 4	+	-	-
2 & 6	+	-	+
3 & 4	-	+	-
3 & 5	-	-	+
3 & 6	-	+	+
4 & 6	-	-	+
5 & 6	-	+	-
6 & 7	-	-	-

- Visual and motor cortex
    1. Torque task with visual feedback and Relax task without visual feedback (**3 vs 6**)
- Somatosensory, visual and motor cortex
    1. Torque task with visual feedback and Rest task without visual feedback (**1 vs 6**)
- Different motor cortex activation due to different muscle activation
    1. EMG task and the torque task with visual feedback (**6 vs 7**)

The last contrast (the torque task with visual feedback contrasted with the EMG task) is hypothesized to not be different, due to the macro scale of measurements compared to the difference in muscle activation as both are regulated by the same cortex patch. An overview of all contrasts can be found in Table 1.

2.4.2 Wrist Perturbation

When system identification techniques are applied to investigate the dynamic behaviour of a system, the in- and output signals are measured to assess the impact of the system on the output signal [41]. As can be seen from Figure 2, the EEG data is extracted from a closed loop system. To identify the dynamics of the wrist and the interaction with the Central Nervous System (CNS), such as causality, linearity and others, an external input signal needs to be designed. A well

designed input signal allows for a quick analysis of the dynamics of the system. A well designed input takes into account the bandwidth of the system perturbed, the possibility of detecting non-linearities, sample frequency and period length. If the frequency content of the applied perturbation is known, the impact of the corticomuscular system from this perturbation on the brain can be extracted from EEG data.

fMRI has a poor temporal resolution, due to the slow reaction time of the hemodynamic system. The increase of the BOLD signal in response to an increase in the metabolism of the neuronal cells of a cortical patch is delayed by a few seconds [29], while electric activity of the cortical patch reacts fast (milliseconds). The impact of the fast movement of the manipulator can only be assessed a few seconds after application. Hence, quick properties of the physiological system can only be assessed with EEG, which shows why EEG can be more informative than fMRI.

Different perturbation design philosophies were considered to enhance the data gathered during experiment execution. These different philosophies were:

- a multisine perturbation based on the Reduced Power method [34],
- a multisine perturbation based on odd multiples of the base frequency,
- a multisine perturbation based on a controller settings (Kp), frequency and amplitude sweep of MR PoPe,
- a transient perturbation based on simple (anti)clockwise movements, also called Ramp-and-hold

The first three methods are based on a perturbation created with known frequency content. The perturbations consisted of multiple frequencies, each with a certain power and random phase. These perturbations are known as multisines. Due to the non-linear dynamics of MR PoPe, the output velocity disturbances have a non-linear response when compared to the input velocity vector. The output of the created perturbations have a low correlation with the input signal time representation. These perturbations were deemed either not exciting enough or impractical to use due to their methodology. Hence, the application of the first three perturbations was not viable.

Hence, the participant had to interact with the robot while a transient perturbation was present. This perturbation is a Ramp-and-hold perturbation. A Ramp-and-hold perturbation means the wrist is moved to one position (flexion), held there for a certain amount of time, and then moved to another position. The wrist movement lasted for 0.2 seconds for both flexion and extension. The range of motion was 0.8 radians. For EEG, the held amount of time is the minimum amount of time for the brain to process all the information gained from the movement, which is 2 seconds. Another extra uniformly chosen random time delay between 0 and 0.3 is added to the wait time to attenuate a learning curve and make the perturbation unexpected. During one trial, 11 wrist flexion and extension movements occur. The first of which needs to be removed, because the perturbation needs to settle. This results in a task time of 48 seconds.

The most important aspect of this Ramp-and-hold perturbation is the velocity profile used to move the wrist. This profile needs to be constant over trials [4, 1].

Experimenting with the participant was performed as follows. The experiment was first explained to the participant. Questions about the experiment were answered fully. Hereafter, the maximum torque during flexion and extension and the EMG during maximum co-contraction generated by the participant were captured. Each was measured thrice, of which the maximum was gathered. These were then used for biofeedback in the training trials. The participant trained each task at least once. Training could be extended per request of the participant. The EEG data were acquired by giving the task trials in a random order. Each task trial adhered to one of the task settings, explained in Section 2.4.1. Each task was supplied twelve times in total. Each task trial consisted of ten usable flexion and extension movements if wrist perturbation was present. Otherwise, a task block lasted 48 seconds without perturbations, with triggers set at a temporal resolution equal to tasks with wrist perturbations. The amount of task blocks and the amount of perturbations per block result in 120 epochs per task (flexion and extension). Randomizing the tasks dissipated dullness, keeping the participant alert and engaged.

2.4.3 Visual Feedback Design

Participants were shown real-time feedback on their performance via a screen. Only the torque and EMG tasks required performance feedback. No performance feedback could be given for the relax and rest tasks, as the participant had no target torque or EMG activation, so a non-timelocked multisine feedback was generated (explained in section 2.5.1). This feedback was not time-locked, meaning the visual feedback was started at a different time index in a multisine period at trigger onset. Hence, the average of all trials contains a random phase per frequency for visual feedback. As the visual system is non-linear [40], the power of the incoming frequencies would also be distributed to other frequencies.

The torque instructed to be applied to MR PoPe by the participant during torque tasks was a continuous flexion torque of the wrist. As the direction of this torque was set, the only property varying is the amplitude of the torque. Muscle activation also has the property that, once filtered, only the amplitude matters. Hence, the visual feedback only needed to display

the amplitude of torque or muscle activation. The direction of the moment generated during the torque task was set to only give feedback when a positive torque (flexion moment) is generated. Negative moments (extension moments) are set to zero. Otherwise, the participant could erroneously interpret the task instruction and apply extension moment instead of the instructed flexion moment.

The visual feedback is a yellow circle on a dark blue background (fig. 3). Suppose the amplitude of the selected biofeedback grows (more flexion torque/activation of the muscles), the circle diameter increases. The circle shrinks when the amplitude decreases. An increased yellow circle increases the intensity of light as compared to a dark blue background. As the tasks without visual feedback lack such a light source, the contrast should be able to localize differences between these brain states. The torque and muscle activation required from the participant was captured in a red ring. The participant needs to keep the outer edge of the circle inside the red ring. The red ring denotes the target biofeedback ±10%. A black cross was presented in the middle of the circle. The participant was instructed and trained to focus on the cross to minimize eye movement.

2.5 Data Processing

2.5.1 Biofeedback Processing

As stated in section 2.4.3, the feedback to the participant depends only on the amplitude of the torque supplied or the amplitude of the filtered EMG data. Hence, only a target torque and EMG amplitude need to be set. The EMG and torque data is acquired at 2048 Hz.

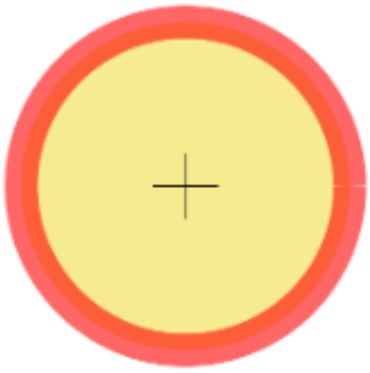

Figure 3: The visual feedback for the participant. The yellow circle grows with torque and EMG input (dependent on the task). When a relax or resting task is presented with visual feedback, the circle's radius is determined by a multisine. The background of the circle is dark blue for a high contrast (not shown). A black cross was placed in the center of the circle. The participant was trained to focus on the cross to minimize eye movement.

The target torque for the participant is 20% of the participant's MVC. If the target torque for the participant is higher than 0.8 Nm, the target torque is set to 0.8 Nm, due to the limitations of MR PoPe. MR PoPe can only deliver a torque of 1.2 Nm [3]. The target torque is enough to elicit an ERP [52].

The fed-back torque data to the participant is the average of all data collected during the last screen update cycle normalized with the target torque. The screen update rate was set to 30 Hz. Flexion torques were set as positive. If the total normalized torque was negative, the circle's diameter was set to 0 to prevent giving feedback about torques in the wrong direction.

The EMG task target is the combination of the activation of both measured muscles. The maximum EMG for both flexion and extension muscles is determined during a co-contraction test. During the co-contraction test, the participant was instructed to maximally contract the muscles in the forearm, while still being able to move the wrist freely. The result is high-pass filtered (10 Hz, third order), rectified and then low-pass filtered (5 Hz, third order). The maximum value for both muscles after filtering is the maximum EMG value. During the task, the participant needed to achieve 20% EMG output per muscle of their relative maximum EMG. The red ring indicates the summed up 20% of the maximum of both muscles.

The fed-back EMG data during the task depended on data acquired during previous screen updates. A 1-dimensional digital filter (3rd order) was implemented as online filtering. At the end of a screen update, the last EMG data point was extracted for both muscles. This data point was filtered with the last data points of the previous three screen updates. The filter pipeline was identical to the co-contraction test, meaning the data is first high-pass filtered at 10 Hz, rectified, and then low-pass filtered at 5 Hz. Finally, the filtered data were normalized with the target muscle activity for each muscle.

For the relax and rest task, the visual feedback was decoupled from the torque and EMG measurements of the participant. During these tasks, the visual feedback shown was a multisine consisting of the frequencies $f_i = 3, 7$, and 11 Hz constructed as in Equation 1 with a random phase per frequency θ_i. The multisine was not time-locked, meaning the visual perturbation started at random time points in the multisine for each trial. This means the multisine had a random phase per period.

$$y(t) = 1 + \frac{\sum_{i=1}^{3} sin(2\pi t f_i + \theta_i)}{3} \tag{1}$$

2.6 Signal Processing

The global data processing steps from raw data until Source Localization (SL) with EEG can be seen in Figure 4. Two important data processing steps are taken before EEG SL is performed. The first steps is

preprocessing the EEG data, which can be found in Section 2.6.1. Hereafter, the steps taken to create a leadfield from MRI and electrode locations are determined (section 2.6.2). Finally, the processing steps for EEG SL are described in Section 2.6.3. EEG data was preprocessed with EEGlab [11]. Leadfield creation and SL were performed with FieldTrip [38].

2.6.1 EEG Preprocessing

Before SL could be performed on the EEG data, it needed to be cleaned. Cleaning of the EEG data means the data is filtered, bad channels are removed from the electrode distribution, and muscle activity and eye movement are to be removed from the EEG data. Furthermore, the data needed to be cut up in periods of

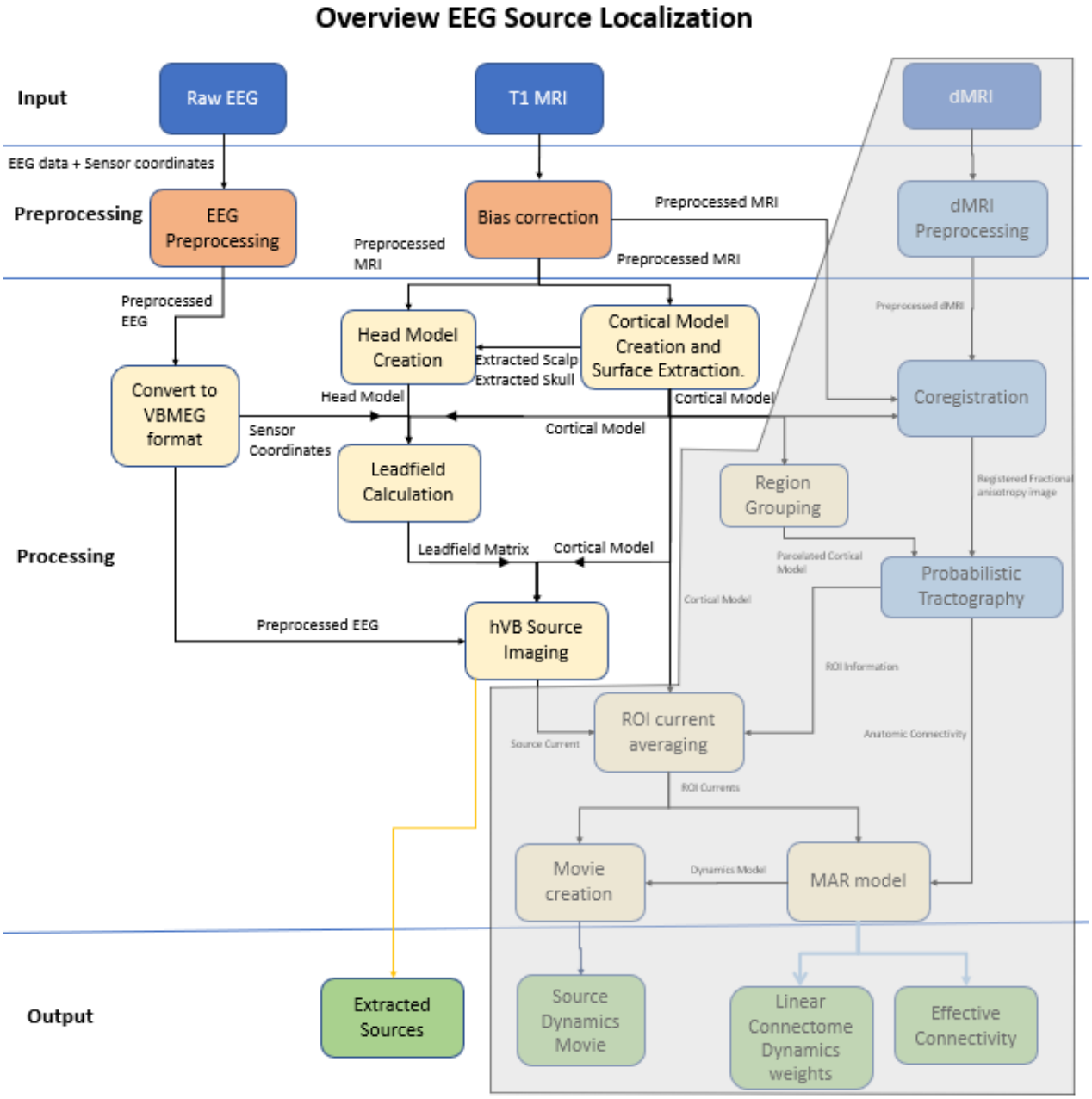

Figure 4: Schematic overview of the EEG, fMRI, and Diffusion Tensor Imaging (DTI) (dMRI in the overview) processing for source localization and ultimately visualizing the flow of Action Potentials (APs) in the brain. All processing steps covered by the grey box are not used in the current data processing, but will be used in a future processing pipeline. The EEG data is first cleaned in the preprocessing step. The structural MRI is corrected for the bias field. From the structural scan, a headmodel and a sourcemodel were created. If no scan is available, a standard head- and sourcemodel are used. These two models, together with the electrode locations, create the leadfield. Then, the leadfield, the sourcemodel and the EEG data are used to derive the source distribution over the brain by applying a SL algorithm. The block model mentions the VBMEG (hVB) method [43], but any source localization algorithm can perform the localization.

interest and assigned to the right task based on trigger data gathered from MR PoPe. All these steps encompass EEG preprocessing. The EEG data was acquired at a sample rate of 2048 Hz, and was preprocessed according to Figure 5.

The data was first demeaned. Hereafter, the triggers were sorted. These triggers were assigned to the different tasks performed, and whether the wrist movement was flexion or extension. In the following step, bad channels were removed. Bad channels were identified based on visual inspection. A band-pass filter between 1 and 200 Hz was applied. A notch filter is applied at 50, 100, and 150 Hz to remove line noise. The data is downsampled to 512 Hz. Hereafter, the data is divided into epochs based on the triggers sent by MR PoPe. The epochs are selected from -1000 to 1500 ms after trigger onset. These epochs were assigned to their respective task by identifying the trigger voltage. Bad epochs were removed. Lastly, artifacts such as eye blinks and muscle activity were removed from the EEG data using ICA. EEG sensor locations were included in the pre-processing stage to apply ICA artifact removal. Including the electrode locations allowed to find the distribution of the weighing matrix over the scalp and identify artifacts based on said distribution.

2.6.2 Lead Field Creation

Before SL can be performed, a leadfield needs to be created according to Figure 6. The leadfield describes the projection of activity per source node to each electrode. A Boundary-Element-Method (BEM) headmodel [15] was chosen for this project. The MRI was segmented into three parts: brain, skull, and scalp. The conductivities of each tissue were set to 0.33, 0.0042, 0.33 S/m, respectively [8]. The source space is created by overlaying the brain volume with a cubic volume filled with source nodes 7.5 mm apart. Source nodes within the volume are viable for SL, while nodes outside of the brain volume are not processed. The head- and sourcemodel are then combined with electrode locations to create the leadfield. No MRI data was available for participant 001 as no MRI scan was made due to time constraints. Hence, the measured electrode positions were morphed to fit the template MRI and electrode location data from Fieldtrip by morphing according to the fiducial markers.

2.6.3 EEG Source Localization

Source localization is performed on the cleaned ERP's. Three different source localization pipelines were constructed to assess the activation of cortex areas (fig. 7). These pipelines were:

1. MNE source localization (dynamic Statistical Parametric Mapping (dSPM) method implementation [9]) on the individual task ERP's

2. Contrasting MNE source localizations between two tasks based on their respective ERP's

3. DICS source localization [16] on a contrast between two tasks based on the wavelet transformation of their respective ERP

The leftmost pipeline is the source localization for individual tasks. First, each epoch is shortened to -500 until 1500 ms after trigger onset to eliminate overlap between epochs. Hereafter, Minimum Norm Estimation (MNE) SL is performed for each time index for the entire average epoch. As such, each time index contains an individual source estimate. Each source estimate represents the source activity normalized with the rest task covariance, without visual feedback. The source space where sources occur is typically divided into discrete elements, with dipole components representing the local current dipole within a small region. The EEG data acquired from these dipoles is described by (eq. (2)):

$$\mathbf{x}(t) = \mathbf{A}\mathbf{y}(t) + \mathbf{n}(t), \tag{2}$$

where x represents the gathered EEG data at each electrode, $\mathbf{A}$ is the leadfield matrix, y is the dipole strength, and n is additional noise from various sources. Source estimates are then calculated multiplying EEG data with a linear operator $\mathbf{W}$ (Equation (3), equation three from [26].

$$\hat{\mathbf{y}}(t) = \mathbf{W}\mathbf{x}(t), \tag{3}$$

where $\hat{\mathbf{y}}(t)$ are the source node activity estimates, and $\mathbf{x})(t)$ is the EEG data. The source activity estimates optimeze the amplitude of the dipole, as well as the orientation, as no orientation was introduced. The linear inverse operator is created in the following way (Equation (4), equation five from [26]):

$$\mathbf{W} = \frac{\mathbf{R}\mathbf{A}^T}{\mathbf{A}\mathbf{R}\mathbf{A}^T + \lambda^2\mathbf{C}}, \tag{4}$$

where $\mathbf{C}$ and $\mathbf{R}$ are the rest task and source covariance matrices, respectively. λ is calculated with respect to SNR, which equates to eq. (5) (equation 6 of [26]):

$$\lambda = \frac{trace(\mathbf{A}\mathbf{R}\mathbf{A}^T)}{trace(\mathbf{C}^* SNR^2)}, \tag{5}$$

where SNR was set to 5, as many evoked response experiments reflect that value [26]. Hereafter, each SL was rest task normalized by applying eq. (6) (equation 6 [26]).

$$z_i(t) = \frac{w_i \doteq x(t)}{\sqrt{w_i C w_i^T}} \tag{6}$$

Dividing the estimated total dipole strength with the predicted standard error (the rest task contains no data of interest), a normalized dipole strength $z(t)$ is obtained at location i.

The middle pipeline estimates the contrast between two tasks and is the SL of interest when compared to fMRI in the time domain. First, the amount of trials used for significance testing is equalized, meaning that if one trial contain 109 measurements

and the other 121, the latter has 12 random trials removed to limit bias in the significance estimation.

Hereafter, cluster based non-parametric permutation tests were performed to assess significant differences between the ERP of the trials to be contrasted [32]. Non-parametric statistical testing is performed as follows:

1. The set of trials adhering to two different experimental paradigms are collected.
2. Create two equally large datasets of randomly selected trials from the data pool.
3. Calculate the test statistic on this random partition.
4. Repeat steps 2 and 3 a large number of times and construct a histogram of the test statistics.
5. From the test statistic that was actually observed and the histogram of step 4, calculate the proportion of random partitions that resulted in larger statistic that the observed one. This proportion is called the p-statistic.
6. If the p-value is smaller than the critical alpha level ($\alpha = 0.05$), conclude that the data in the two experimental conditions are significantly different.

The test statistic from step 3 is created as follows.

1. For every (time, electrode) pair in two experimental paradigms, calculate the t-statistic between the two samples.
2. Select t-statistics that exceed a threshold. Here, a two-sided t-test at alpha level 0.05 is performed. The threshold is the 97.5 percentile.
3. Cluster samples based on spatial (, spectral) and temporal adjacency.
4. Calculate the cluster statistic by taking the sum of t-values in a cluster.
5. Each cluster is represented on each electrode ERP data, where each cluster has a different t-test sum.

The randomization is performed a hundred times to construct the histogram of test statistics. A two-sided t-test at alpha level 0.05 is performed. The threshold is the 97.5 percentile. Temporal and spectral adjacency are easily defined as the next or previous time index or frequency band. Spatial adjacency was determined by triangulation of the electrode locations. Each electrode defined as a neighbor could add to the cluster of an electrode. The electrode positions are first projected on a 2D-plane in the x, y and z directions. Then, neighbors are determined by Delaunay triangulation in each 2D-plane.

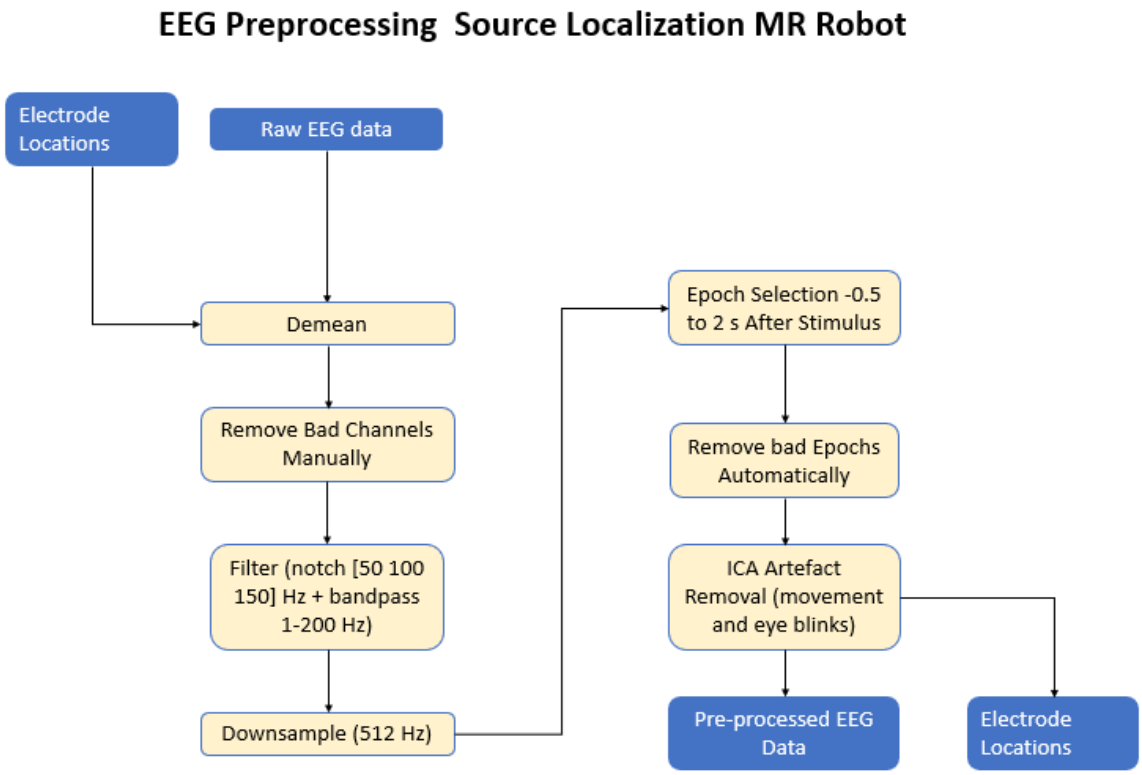

Figure 5: The figure gives a schematic overview of the EEG data pre-processsing. The data was first demeaned, after which bad channels were removed based on visual inspection. A band-pass filter was applied between 1-200 Hz, and notch filters were set at 50, 100, and 150 Hz. The data was downsampled to 512 Hz to save memory. Epochs were selected based on trigger onset, with time windows -1000 ms to 1500 ms after trigger onset. Bad epochs were removed, and lastly, artifacts such as eyeblinks and movement were removed by applying ICA.

The time indices within these significant time windows will be extracted to evaluate the accuracy of the SL. The SL for each individual task is loaded from the individual task Source Localization (SL) pipeline. The time index with maximum difference between ERPs is chosen within each significant time window, and the SL for that time index is extracted. As the magnitude of the source node is of importance, it can be taken as absolute. The tasks are then contrasted in three ways:

- subtraction of the SL of the contrasting task from the task of interest (eq. (7)),

$$SL(t) = SL_i(t) - SL_c(t) \tag{7}$$

- division of the SL of the contrasting task from the task of interest and coverting to Decibel (eq. (8)),

$$SL(t) = p * log10(\frac{SL_i(t)}{SL_c(t}), \tag{8}$$

where p equal 20 for ERP SL and 10 for TFR SL,

- a combination of the previous two called the iscdc contrast (eq. (9)).

$$SL(t) = \frac{SL_i(t) - SL_c(t)}{SL_c(t)} \tag{9}$$

SL_i indicates the magnitude of interest, and SL_c is the magnitude to be contrasted with. It is not yet known which contrasting method is preferred for each pipeline.

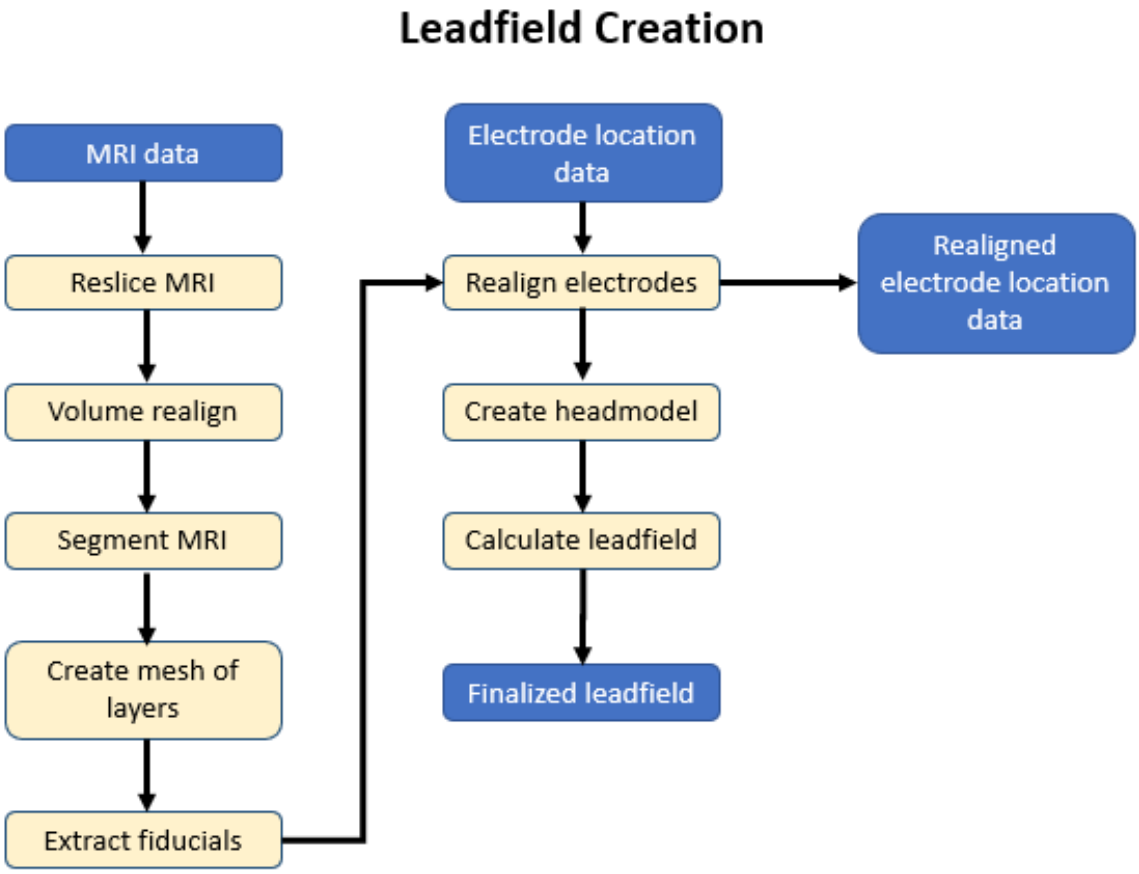

Figure 6: A block diagram visualizing the steps taken to create the leadfield used for SL. The MRI was first resliced such that the volume is made of 256 × 256 × 256 voxels. Hereafter, the MRI is realigned to the RAS coordinate system (Right, Anterior, Superior for the x, y and z axes respectively, origin at the anterior commissure). Hereafter, the MRI was segmented into three tissues for the BEM head model (brain, skull, scalp) and a mesh was created at the border of all three tissues. The fiducials are extracted from the scalp mesh and used to realign the electrode locations to the MRI voxels. A headmodel is created using the bemcp method from Fieldtrip, where the conductivities of each tissue were set to $0.33, 0.0042$ and $0.33 S/m$ for the brain, skull and scalp respectively [8]. Hereafter, the sourcemodel is created by distributing source nodes throughout the grey and white matter with an internode distance of 7.5 mm. The nodes are placed by filling a cube volume over the inner headmodel volume, with source nodes at the inter node distance from each other. Any nodes outside the inner headmodel volume were not taken into account during SL. Lastly, the leadfield is created by combining the headmodel, sourcemodel and the realigned electrode locations. Participants 002 and 022's sourcemodel contains 3624 source nodes, while the sourcemodel of participant 001 contains 3630 source nodes.

Contrasting the ERP SL indicates that the amplitude or source power at a source node has changed in comparison to the source distribution of the task to be contrasted with. A positive difference in the case of subtract would indicate that the extracellular fluid is more positively charged in comparison to the task that was contrasted with. The function of the more positive charge is not known, as a lot of chemical processes are executed synchronously.

ERP SL contrasts are visualized at the time index in a significant different cluster of time indices, where the largest voltage difference between the contrasting task ERP's occurs at electrodes of interest. The time index must be in a significant different cluster, as significant testing shows that the data from the ERP's at these clusters cannot be drawn from the same data pool. The largest difference between ERP's was chosen, because it implies the largest projected difference between source distributions between the contrasting tasks. The electrodes C3 and OZ were chosen as electrodes of interest, as they lie above the sensory-motor cortex and the visual cortex respectively. The SL at the selected time index is interpolated over the MRI of the participant and visualized by transversely slicing the interpolated data.

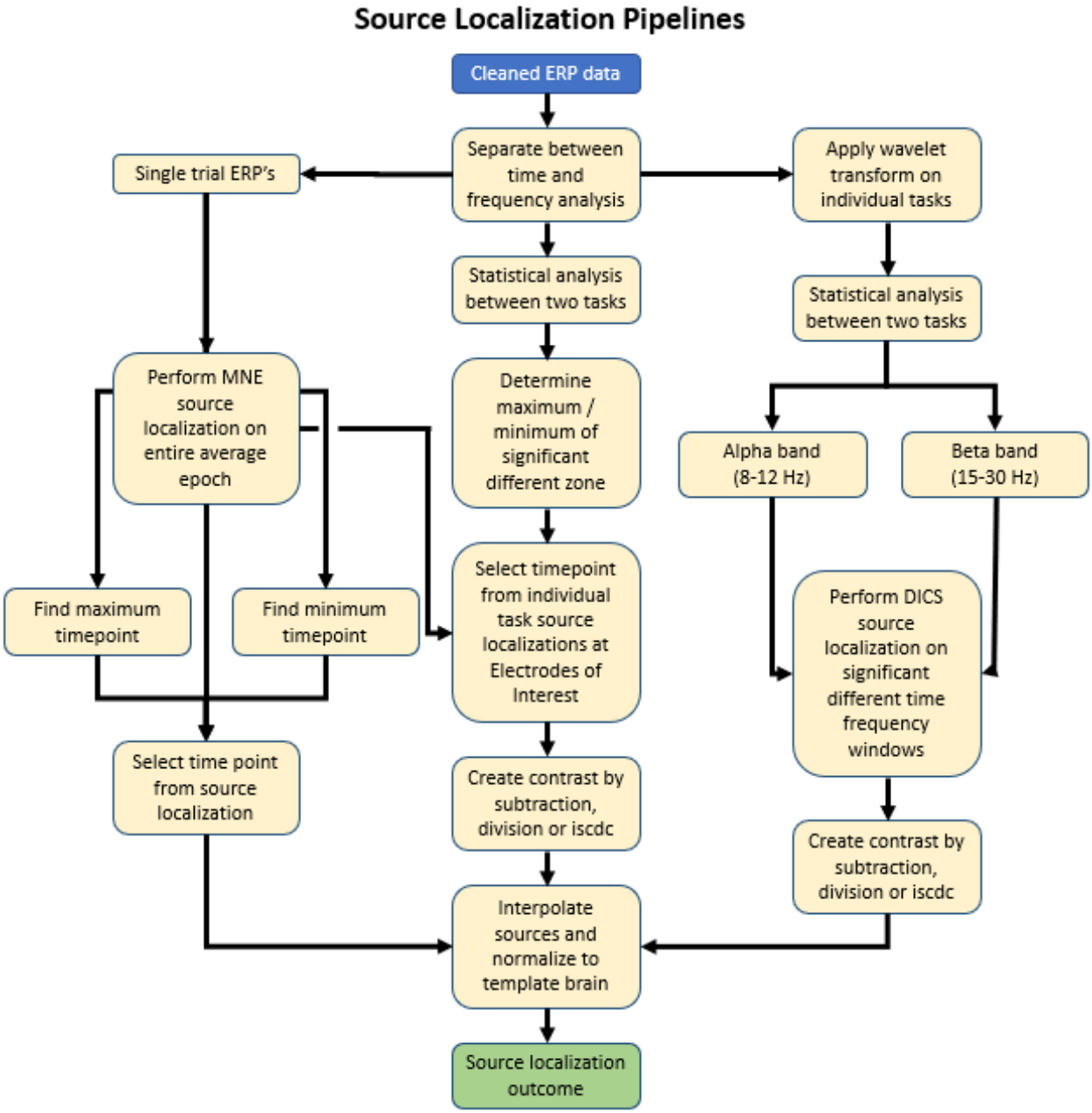

Figure 7: A schematic overview of the various source localization pipelines. The left column shows MNE source localization for single-task ERP's. The middle column shows MNE source localization for contrasting two tasks with ERP's. Data from the first pipeline is used in the second pipeline, as indicated by the crossing arrow. The last column shows source localization using TF windows and DICS. For each source localization, the created headmodel and leadfield were created according to Figure 6.

The Time-Frequency Response (TFR) pipeline works approximately the same as the time domain contrast SL, except for a different data representation. First, significant TF windows need to be created to apply TFR SL. The ERP's were converted to time-frequency data from 3 to 50 Hz at a 1 Hz resolution by applying Morlet wavelets [49]. The number of cycles increased incrementally for 3 to 50 Hz from 3 to 10 cycles. Hereafter, the amount of trials in each task was equalized. The frequency window (either alpha (8-12 Hz) or beta band (15-30)) for significance testing is selected. These bands reflect cortical visual [10] and motor [33] activity, respectively. Again, cluster based permutation tests are performed to identify significantly different time-frequency windows. Significant TF windows are selected from electrodes C3 (motor cortex) and OZ (visual cortex).

To perform SL, all tasks are again converted from the time-domain to frequency data using the mtmfft method in Fieldtrip for each TF window with a length larger than 0.2 s for the alpha band and 0.13 s for the beta band, due to the smoothing constraint of the mtmfft method. The mtmfft method removes the time aspect of the Wavelet analysis and concentrates all power from the significant TF window in a single value for each frequency band, while also calculating the cross-spectral density between all electrodes. For SL, a single frequency needs to be selected, and the smoothing constraint ensures that all power from the frequency window of interest is concentrated in the single frequency selected for SL. The frequency used for SL is always the frequency at the middle of the frequency band (10 Hz for alpha and 22.5 for beta). The entire frequency band is used for SL, even when not indicated by the TF window. A common spatial filter is created among all tasks (including Rest) by performing SL by applying the DICS algorithm. The common filter is then used to apply SL for the tasks of interest and rest. The SL are normalized with rest. The tasks are contrasted in an equal fashion to the contrasting in the middle SL pipeline, and visualized on the MRI of the participant.

The DICS algorithm [16] uses the estimation of the cross spectral density $\mathbf{C}(f)$ of a frequency band centered at f to perform SL. The cross spectrum estimates between four tangential source combinations at locations $\mathbf{r}_1$ and $\mathbf{r}_2$ at frequency f are represented by the 2×2 matrix (eq. (10)):

$$\mathbf{C}_s(\mathbf{r}_1, \mathbf{r}_2, f) = \mathbf{A}(\mathbf{r}_1, f)\mathbf{C}(f)\mathbf{A}^{*T}(\mathbf{r}_2, f), \tag{10}$$

where $\mathbf{A}$ is a linear transformation matrix that, when applied to the data, passes the activity of location $\mathbf{r}$ with unit gain for a specified frequency band, while suppressing contributions from other sources. When $\mathbf{r}_1 = \mathbf{r}_2$, $\mathbf{C}_2$ becomes a 2×2 matrix containing the power estimates (eq. (11).

$$\mathbf{P}(\mathbf{r}, f) = \mathbf{C}_s(\mathbf{r}, \mathbf{r}, f) \tag{11}$$

The power at the source then complies to Equation (12):

$$p(\mathbf{r}, f) = \lambda_1(\mathbf{P}(\mathbf{r}, f)), \tag{12}$$

where λ are the singular values of $\mathbf{C}_s$ and $\lambda_1 \gg \lambda_2$. The dipole power at each source node is then normalized with the power of the resting task (eq. (13)).

$$p_N(\mathbf{r}f) = \frac{p(\mathbf{r}, f)}{p_{Rest}(\mathbf{r}, f)} \tag{13}$$

An increase or decrease for frequency band power at a source node indicates an amplification or attenuation of oscillatory power for sources in that area. No physiological meaning has been found behind the (a)synchronous activity.

The localization of sources will only be evaluated empirically. Due to the limited participant pool, the experiment's parameters can be validated, but no hard conclusions can be drawn about the data. It is necessary to validate if the SL pipelines can differentiate between task executions and localize attenuation or amplification to different cortex patches.

3 Results

Identification of the activation of individual and multiple cortex patches was hypothesized with various contrasts in section 2.4. The contrasting formulae used to contrast between tasks were discussed in section 2.6.3. First, the contrasting method is chosen for the ERP and TFR SL pipelines used to compare tasks (only the middle and left, fig. 7) to reduce the results for source localization. Hereafter, an overview of the outcomes of localization of each functional area is shown, and examples of these outcomes.

3.1 The Contrasting Method

To perform SL, the significant time and TF windows for ERP and TFR SL, respectively, need to be selected. An example of the significant windows for each contrasting SL pipeline can be found in Figure 8.

The SLs are plotted over a transverse sliced MRI scan. The slice on the top right is the most superior slice, while the slice down left is the most inferior slice. Anterior is on the top of each slice, and left on a slice is left.

When localizing in the time domain (ERP), the subtract contrast is the best option for localization. A correct localization of activity for ERP SL is shown in Figure 9, which is created by the contrast subtract. The division method results in focal sources spread throughout the brain, and the iscdc method results in one singular focal source localized somewhere in the cerebrum. Hence, contrasting at the ERP level will be performed by the subtract method.

Localization in the TF domain is performed with the division method. A correct localization using the method division is shown in fig. 10. Localizations for all

three methods appear approximately equal. Localizations for the subtract and iscdc methods appear more precise compared to the division method. Large differences appear however when both power attenuation and amplification are localized in a singular SL. The amplifications fade when division is employed, while these remain when the iscdc and subtract methods are used. Division will be used to evaluate the correct localization of TFR SL.

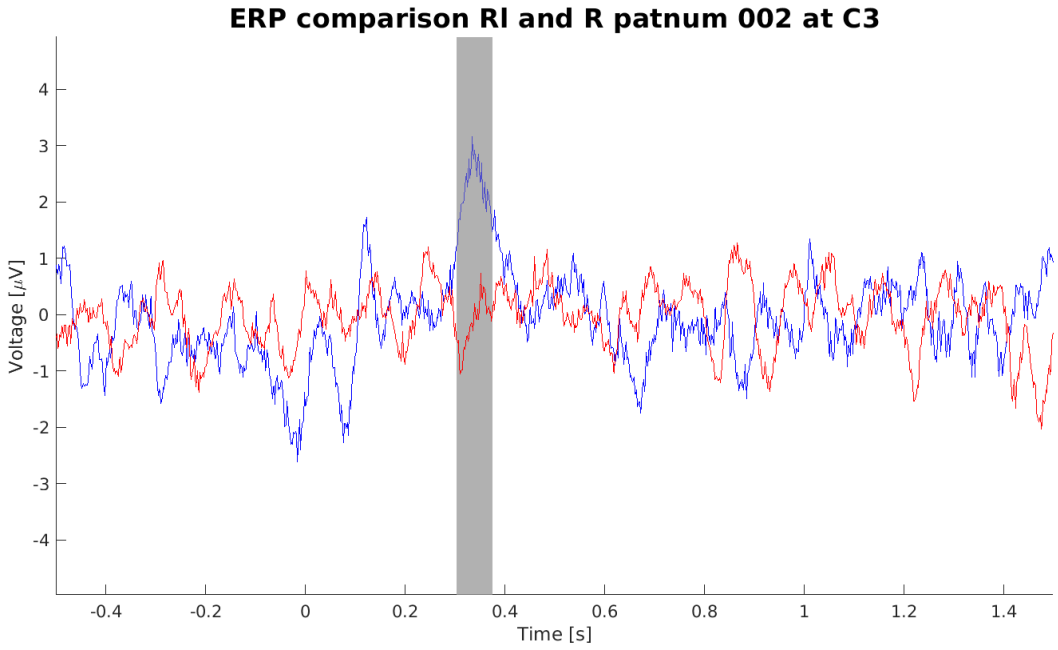

(a) ERP significance testing for participant 002 at electrode C3 for the contrast between the relax task and rest task, both without visual feedback.

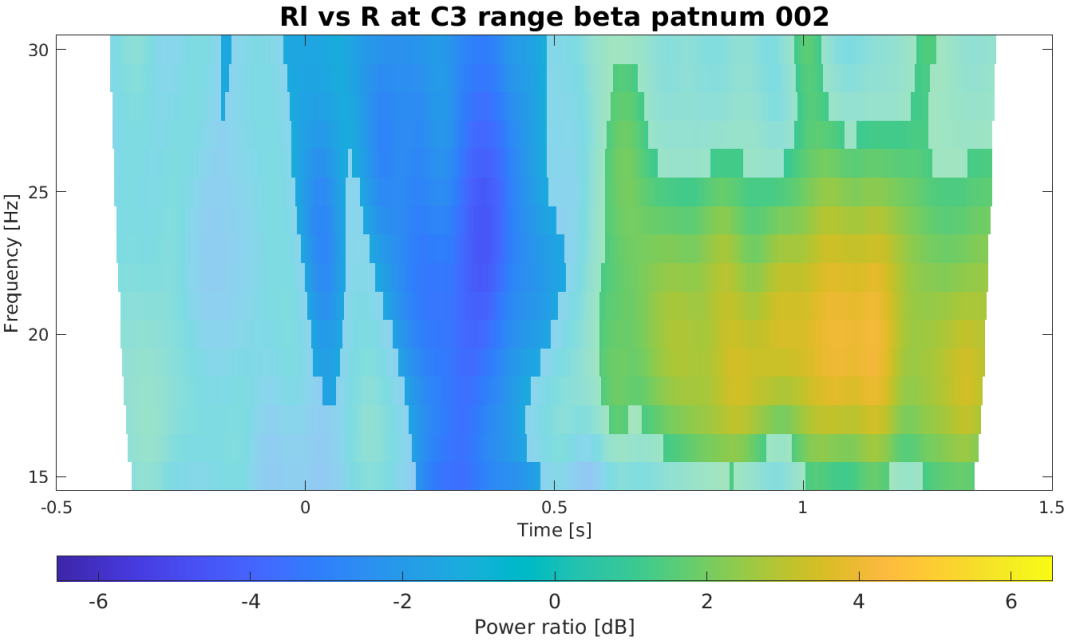

(b) TFR significance testing for participant 002 at electrode C3 for the contrast between the relax task and rest task, both without visual feedback, in the beta frequency band.

Figure 8: Significance testing on both the ERP and TFR level. Significant windows are grey colored on ERP level, while significant TF windows are not bleached. Each ERP grey area has an accompanying SL on the time index with the highest difference between ERPs within the area. Each large enough TF window has an accompanying SL, if the window is temporally long enough.

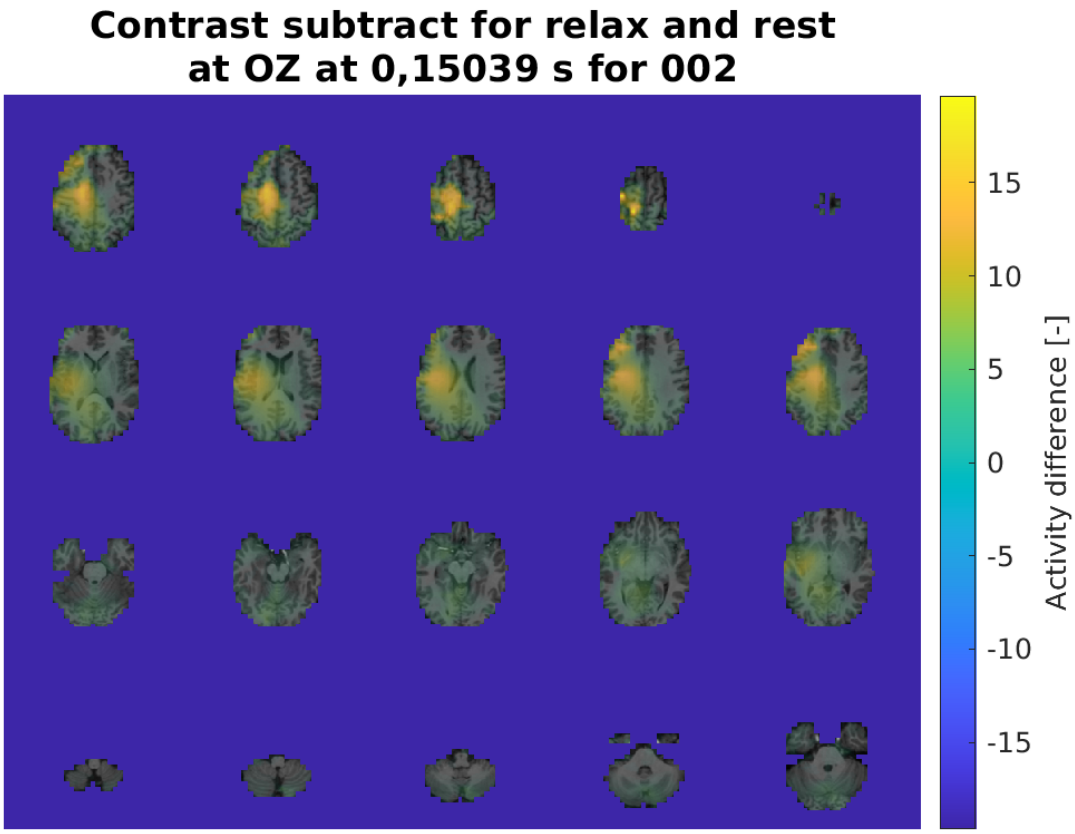

Figure 9: ERP SL at time index 0.150 s at OZ for the contrast relax with rest, both without visual feedback, for participant 002. A positive activity difference is localized to the superior left. The most superior slice is on the top right, anterior is at the top of each slice, and left remains left.

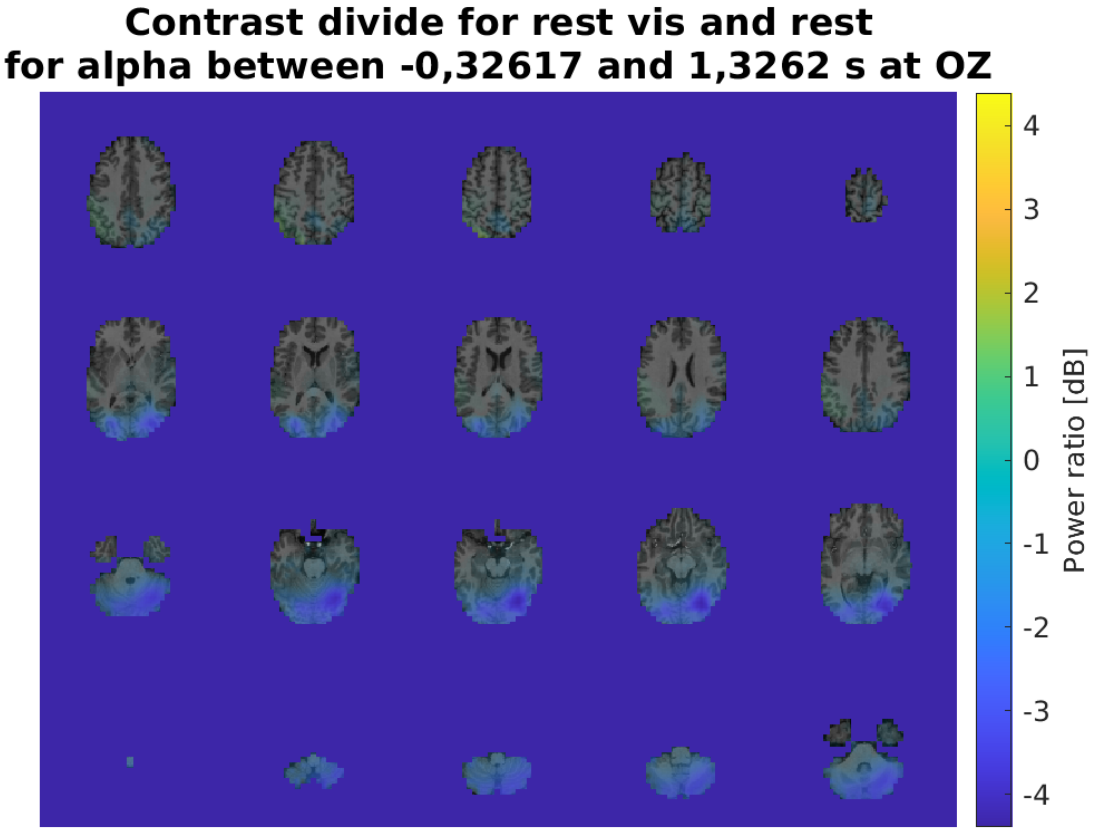

Figure 10: TFR SL from time index -0.32617 until 1.3262 s in the alpha band for electrode OZ for participant 002 for the contrast rest, with and without visual feedback. Power attenuation is localized to the posteroinferior right.

3.2 The Location of Functional Areas

Three individual functional areas are hypothesized to be localized with the current experimental setup. These areas are the visual, somatosensory and motor cortex. The correct localization of these functional areas is compared to Figure 12.7 and 12.8 from Marieb and Hoehn [31]. These figures represent the already established knowledge of functional areas in the human brain and the spread of cortical tissue devoted to each function of the human body.
The visual cortex is located to the posteroinferior of the cerebrum. As such, localization would be deemed correct if localization of activity points to the posteroinferior. However, complex visual processes involve the entire posterior half of both hemispheres. As such, localization of the visual cortex is deemed correct if activity is localized posterior of the brain middle. The primary somatosensory and motor cortex are located around the central sulcus and neighbor each other. As each hemisphere governs the function of the contralateral side, localization of activity is expected to occur in the left hemisphere as the right wrist is moved and used to apply torque. The body map for the somatosensory and motor cortex shows that sensory processing and control of the wrist are superior in the cerebrum. Hence, both the localization of the somatosensory and motor cortex is expected to lead to activity superior in the left hemisphere. The motor cortex should be localized anterior to the somatosensory cortex. An overview of correct localizations can be found at Figure 11. Various outcomes exist for hypothesized and non-hyptothesized functional areas. Results for each possible outcome are shown below.

Correct localization of the somatosensory, visual and motor cortices is shown in Figures 9, 10 and 12. Activity of the somatosensory cortex fig. 9 is clearly located to the superior left of the cerebrum. The visual cortex fig. 10 is localized to the posterior, which is a correct localization. The highest attenuation is localized slightly to the right of the primary visual cortex, and is deemed a correct localization by the previous set standards. Correct localization of the motor cortex is achieved by Figure 12. Power attenuation is achieved superior left in the cerebrum. The time window used for localization is -0.21 until 0.025 s after trigger onset, meaning slight wrist movement contaminates the TF window. As such, a localization to the superior left can only be attributed to the constant torque applied to the manipulandum.

Finally, correct localization can be found at other electrodes, instead of the hypothesized electrode. These are deemed correct localizations. No SL can be performed when no significant time windows can be found in either the ERP or no large enough TF windows can be found in the TFR domain (marked blue in fig. 11).

Previously shown localizations are deemed correct. However, in some settings, SLs are not in line with the hypothesis. Sometimes activity is not localized to the hypothesized location (false positive), non-hypothesized neuronal ensembles become active (false negative), or the activated neuronal ensemble could be explained by the activation of multiple functional areas. For example, a false positive localization of the somatosensory cortex would be the contrast relax and rest, both with visual feedback, for participant 001 at C3 at timestamp 0.152 s (fig. 13). The time stamp matches correct localization for the other participants. However, localization of activity is too widespread and too inferior, and therefore not in line with the hypothesis.

An example of unhypothesized localization activity is presented by Figure 14. Alpha band localization at OZ localizes the visual cortex (power attenuation posterior). However, a power attenuation spike is also localized at the superior left, indicating the somatosensory cortex. These localizations are false negatives.

An example of inconclusive localization is localization of the not hypothesized visual cortex shown in the contrast identifying the motor cortex (fig. 12). Beta power attenuation is localized to the posterosuperior

Activated cortex	Task Contrasts	002 S	002 V	002 M	022 S	022 V	022 M	001 S	001 V	001 M
S	Rl vs R	+			+			0		
S	RlV vs RV	+			+			bd	-	
V	RV vs R		0			0			+	
V	RlV vs Rl	-	+			0			+	
V	TV vs T		+		||	+	||		+	
M	T vs Rl	||		||			0	||	||	||
M	TV vs RlV	||	-	||	||	-	||		||	bd
SV	RlV vs R	+	o+		+	0		0	+	
VM	TV vs Rl		+	bd	||	+	||		||	bd
SM	T vs R	+		+	+		||	||	||	bd
SM	TV vs RV	o+	-	||	+		||	bd		||
SVM	TV vs R	0	+	bd	+	0	||	bd	+	bd
EMG FV	EMG vs TV		-	+			0		||	+

+	hypothesized and active
-	false negative
0	no significance for S
0	no large enough time window for V and M
||	possible activity
bd	false positive
o+	not localized on expected electrode, other electrode localizes correct

Figure 11: An overview of the localizations per task contrast and whether they were deemed correct. Other possible outcomes are: false positive (no activity at hypothesized location), false negative (not hypothesized and active) significance is reached, localization achieved on another electrode, localization is unclear about what is localized. S: somatosensory, V (in activated cortex patches): visual, M: motor, R: rest, Rl: relax, T: torque, V (in task description): with visual feedback.

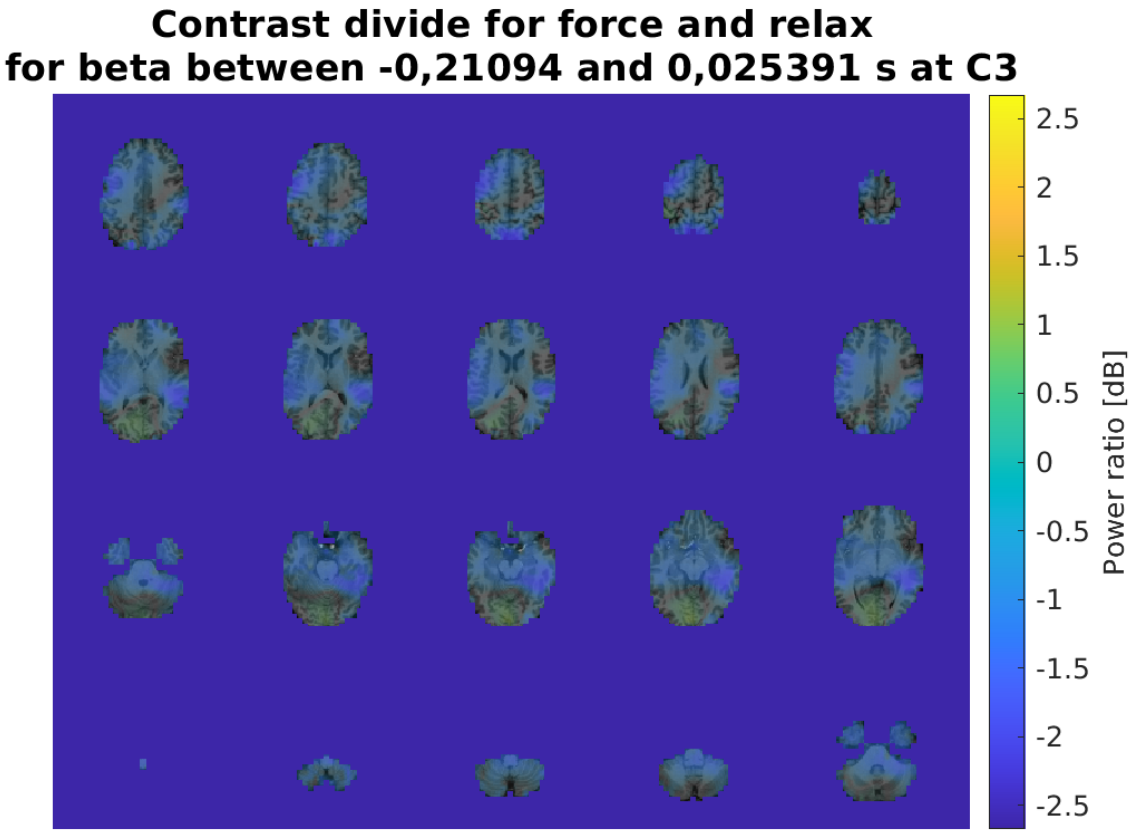

Figure 12: Correct TFR beta band SL for the force task contrasted with the relax task, both without visual feedback. Power attenuation is localized to the anterosuperior left. However, a steep spike is also localized to the posteroinferior, indicating activity to the visual or the somatosensory association cortex, which leads to possible localization of the visual cortex.

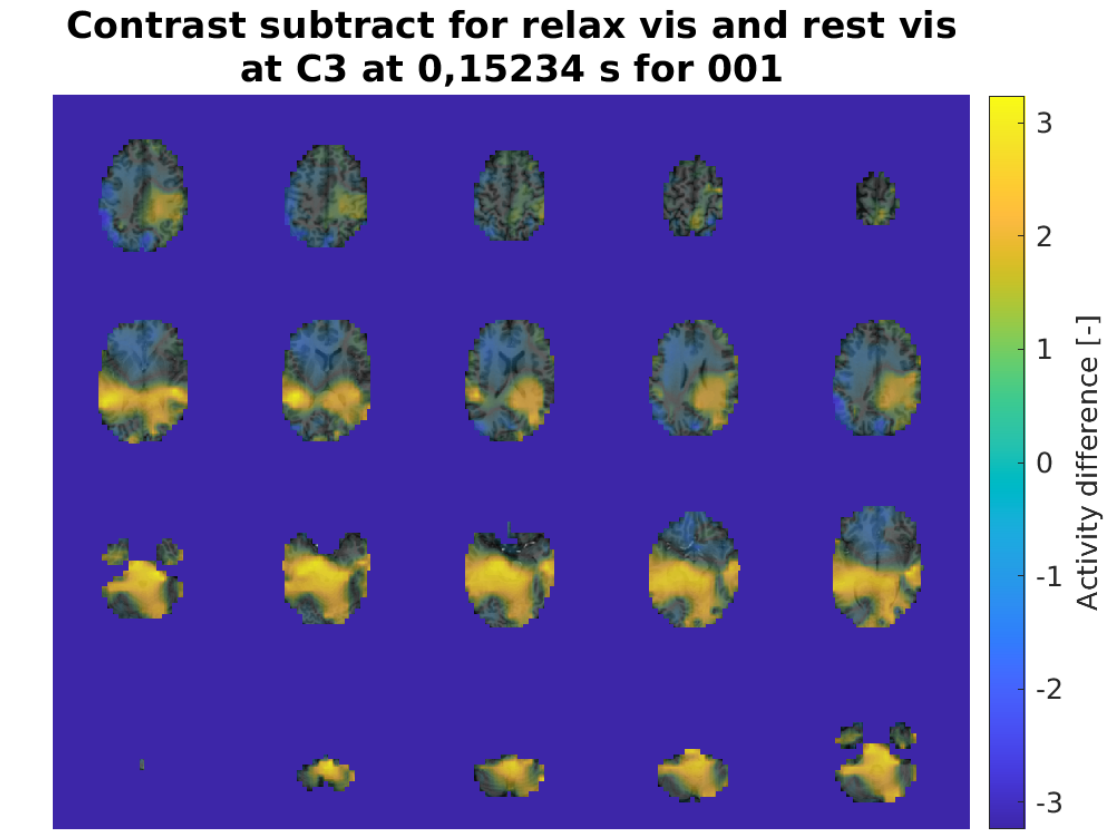

Figure 13: Unexpected (bd) SL for the contrast relax and rest, both with visual feedback for participant 001 at electrode C3. The left somatosensory should be localized in the current contrast. This is an example of a false positive (bd).

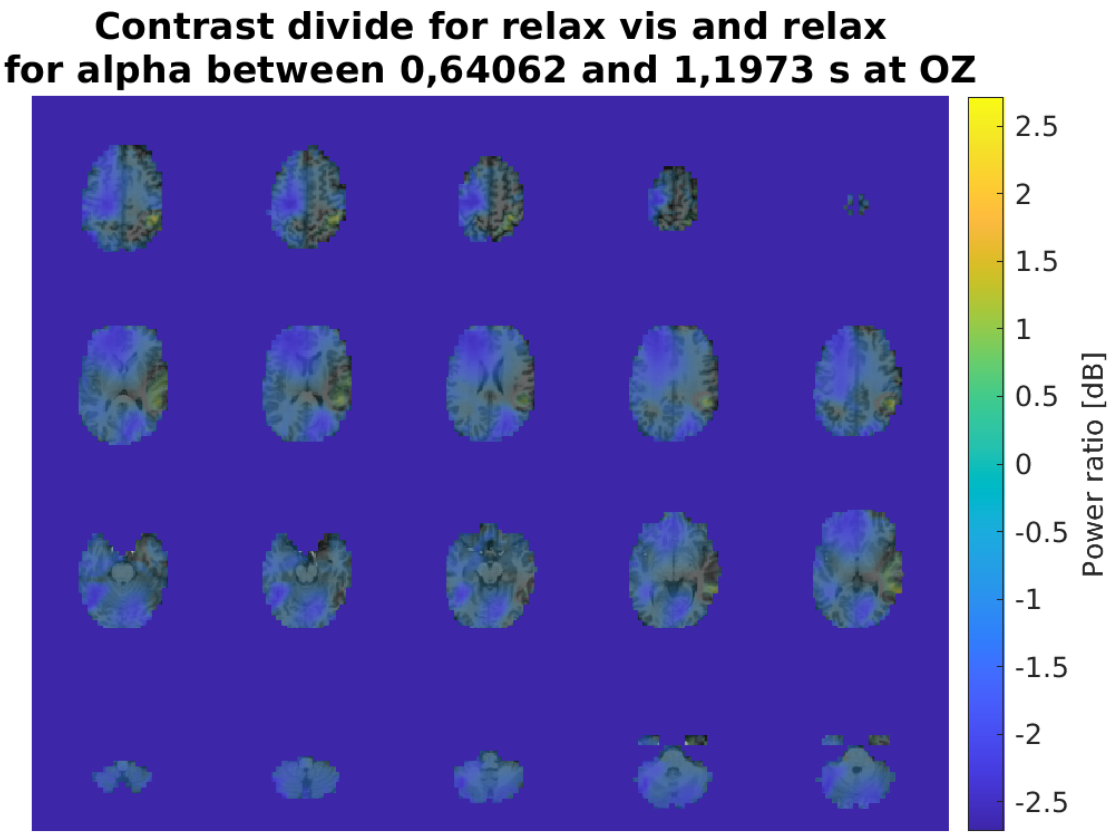

Figure 14: TFR SL for participant 002 at OZ for the contrast relax, with and without visual feedback. The visual cortex is localized as expected. However, a source is also present at the somatosensory cortex (superior left). This is an example of a false negative (-).

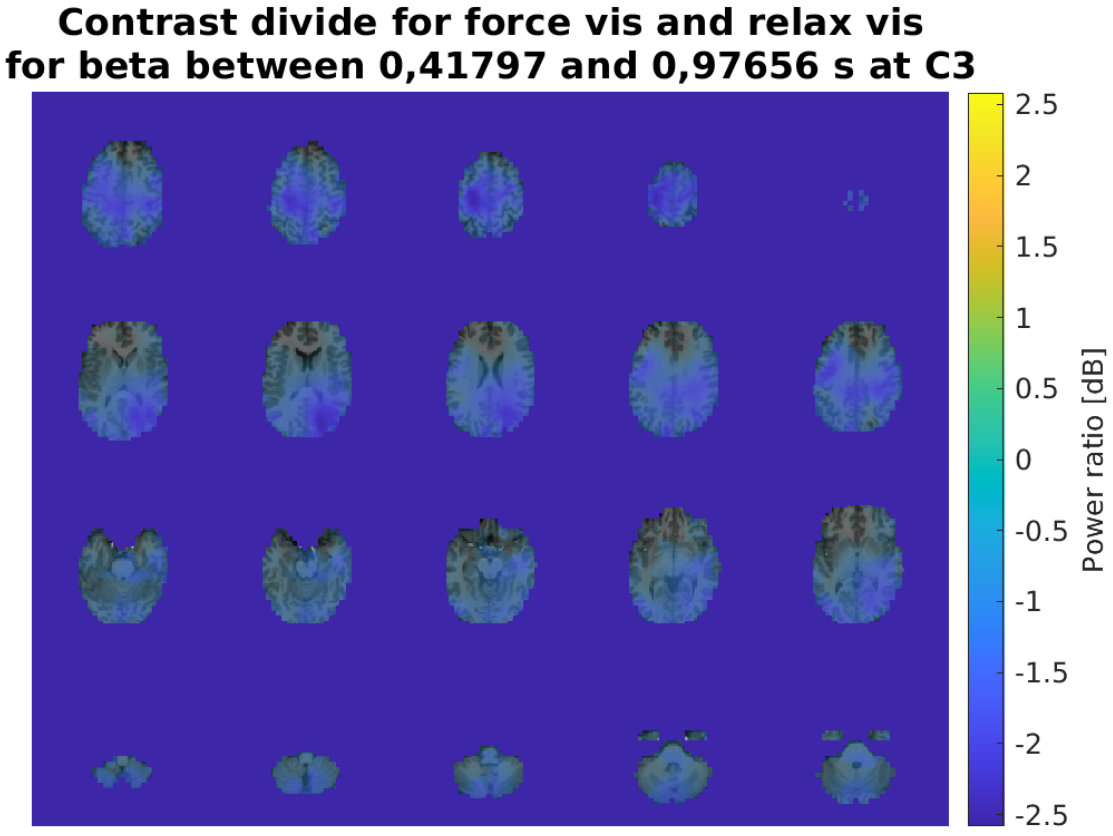

Figure 15: In conclusive localization of either the motor or somatosensory cortex. Beta power attenuation is localized to the superior left. The task localization is however contaminated with wrist movement for both tasks. Localization of the somatosensory cortex can not be excluded from possible functional areas, resulting in possible localization of both functional areas.

side of the cerebrum. The activity appears localized to the visual association cortex. However, as the localization is superior, it could also indicate the somatosensory association area. These visual cortex localizations are performed at the frequency bands used for motor cortex localization (beta band). Such localizations result in a possible activity in the visual area in Figure 11.

Another example of inconclusive localization is the determination of the motor cortex at TF windows after trigger onset. Figure 8b shows beta power attenuation, followed by power amplification for significance testing of the relax task contrasted with the rest task, both without visual feedback. Significance testing for the torque task contrasted with the rest task, both without visual feedback (fig. 16a), shows the same attenuation and amplification trend. However, differences can be seen. The power attenuation window starts before trigger onset for the latter figure. The power amplification window starts later in the epoch, compared to the contrast relax with rest. It shows that continuous application of a torque creates continuous beta power attenuation. However, it is unclear whether the wrist movement or applied torque are mainly responsible for the power differences. Hence, motor cortex localization

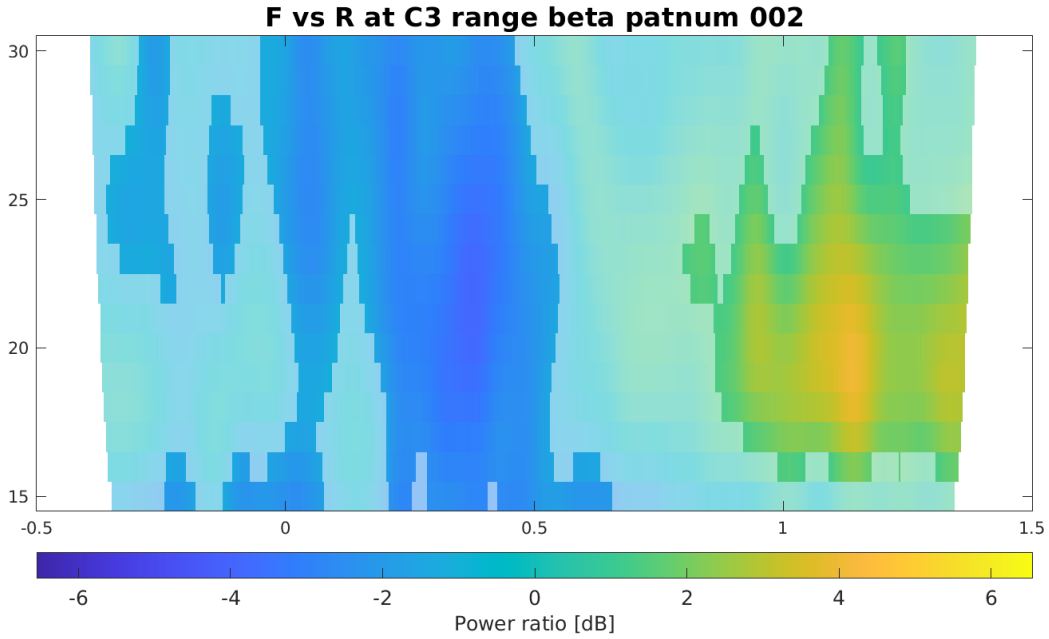

(a) Significance testing for the torque task (F) contrasted with the rest task (R), both without visual feedback.

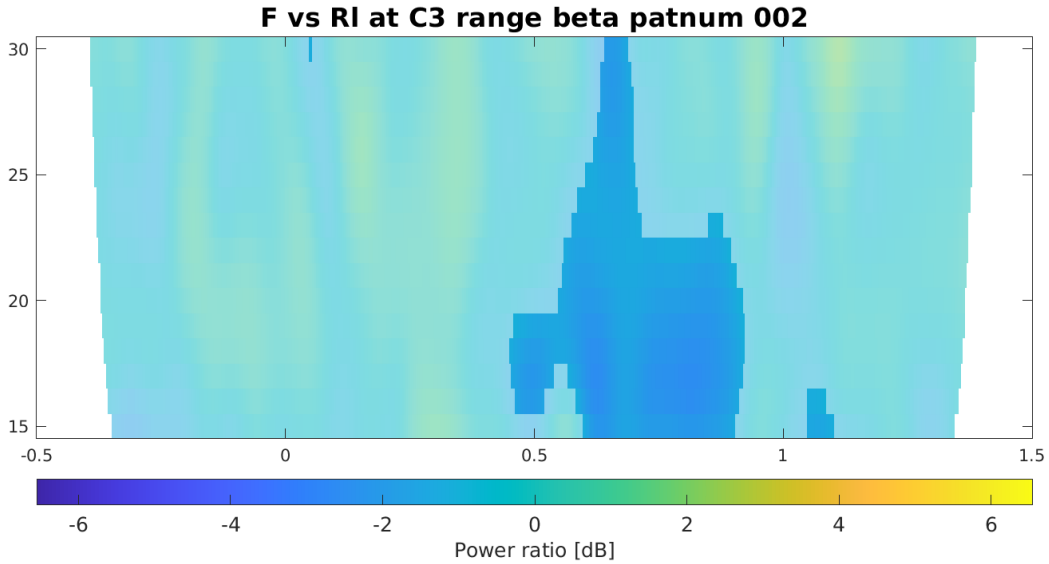

(b) Significance testing for the torque task (F) contrasted with the relax task (Rl), both without visual feedback.

Figure 16: Significance testing for participant 002 in the beta band at C3. Figure 16a has beta power attenuation before trigger onset, indicating the constant torque applied on the manipulandum. The beta power amplification window starts later compared to Figure 8b. Figure 16b shows the difference between the torque and relax significance tests. It shows no difference before trigger onset, indicating no difference in activation. The significant window shows the delay in power amplification caused by applying a torque to the manipulandum.

after trigger onset can be attributed to both the motor and somatosensory cortex, as both neighbor each other. The contrast torque with relax, both without visual feedback (fig. 16b), shows power attenuation from 0.5 until 0.9 s after trigger onset. The question remains if this window is created due to the beta desynchronization of the torque task or the increased power of the wrist movement. Hence, again, localization after trigger onset can be attributed to both the somatosensory and motor cortex. Finally, localization of multiple functional areas does localize the somatosensory cortex, but shows a possible localization for the motor cortex. The motor cortex is possibly localized, due to contamination of wrist movement. However, ERP SL localized the somatosensory cortex correctly and is therefore deemed correct instead of possibly localized.

4 Discussion

First, a recap of the localization of source activities for all pipelines. For ERP SL, the SL per task is calculated. Hereafter, the time index to inspect the localization needs to be determined. For the single task localization, it is the time index with the maximum and minimum for the ERPs at C3 and OZ. For contrasting, it is the time index with the highest difference between ERPs per significant window at C3 or OZ. The SL for the tasks to be contrasted is loaded in, the time index is selected, and the SLs are contrasted according to the subtraction method.

TFR SL localizes activity different. First, each task is a Morelet transformation to create a TF representation of the data. A significance test is performed between the two tasks of interest. This test will inform the SL of the TF window to localize activity on. DICS need the power over the TF window localized into a single frequency. Hence, the mtmfft method is applied to average the frequency band to the center frequency (middle frequency of the frequency band) and to find the cross spectral density between electrodes for the TF window. After SL, the division method is used to contrast between localizations.

4.1 The Contrasting Method

Careful examination of the localization for the somatosensory cortex only (Rest contrasted with relax task, both with and without feedback) in both the ERP and TFR domain shows that different contrasting methods need to be used for each Source Localization (SL) pipeline. As the somatosensory cortex is activated by the right wrist, the source activity should be localized to the left side of the brain ([31]). Where Event-Related Potential (ERP) localization only appears spread out for division and very focal or not existent for iscdc, subtraction provides an answer in accordance with the truth. Only subtraction shows clear localization to the left. While the source activity is spread out over a large volume, only one overarching source can be found.

The contrasting method to be used for Time-Frequency Response (TFR) SL is division. Activity is localized approximately equal across all contrasting methods. When significant power differences in only the positive or negative direction are found between the SL of the task of interest and the contrasting task, these visualisations are almost interchangeable. However, contrasting with iscdc and subtract appears more intense when power amplification is present, and for good reason. Sources visualized by division converted to decibel can attain power $[-\infty, \infty]$. Iscdc has a range of $[-1, \infty]$. The pivot point for both is at 0. Hence, the iscdc contrasting method is not linear, which is why iscdc can show a higher color for power amplification. Subtraction will compare the contrast between tasks with the power in noise. For example, when the torque and relax task are contrasted, subtract will show the following data, due to the normalization step with the rest task (eq. (14)).

$$P_{contrasted}(t, f) = \frac{P_T(\mathbf{r}, f) - P_{Rl}(\mathbf{r}, f)}{P_R(\mathbf{r}, f)} \tag{14}$$

The division with the rest task for the contrast subtract will further complicate the interpretation of localization. Hence, division is preferred over subtraction and iscdc.

4.2 Localization of Functional Areas

As evidenced by Figure 11, localization of the somatosensory cortex was no problem for participants 002 and 022. The localization has a temporal consistency over the participants. Around 0.15 s after trigger onset, a peak occurs at which the somatosensory cortex can be localized. This time index is considerably later compared to Campfens et al. [4], which reports a peak 0.03 s after trigger onset and a long latency peak maximally 0.15 s after trigger onset, but averaged at 0.067 s. The longer long latency response in comparison to Campfens et al. [4] can be explained by the longer perturbation duration (200 ms instead of 50 ms). The peak does not necessarily have to be present at C3, as the somatosensory cortex for participant 002 in the torque task, with visual feedback, contrasted with the rest task, with visual feedback, is localized at electrode OZ at the same time index.

Localization of the visual cortex was more troublesome, but can be concluded successful, as both participant 002 and 022 can locate the functional area when a significant difference is present. However, participant 022 often has no large enough significant TF window to localize the visual cortex. An explanation for this lack of difference between datasets is that the visual feedback does not induce enough activity when switched on.

Localization of the motor cortex is often inconclusive due to contamination of the wrist movement. The constant applied torque generates beta power attenuation over the entire epoch. However, the wrist movement induces beta power attenuation after trigger

onset and follows it up with power amplification near the end of the epoch. A single instance for participant 002 localizes activity to the superior left and at time indices before trigger onset, indicating only the motor cortex.

Localization for participant 001 is less agreeable with the data of the other participants. Localization of the somatosensory cortex is often non congruent with the hypothesis or not significant. The visual cortex is localized correctly more often. The visual cortex is more often possibly localized, when localization is not hypothesized. The motor cortex is always an inconclusive localization, which is in agreement with participant 022.

An explanation for the vast amount of bad localizations of the somatosensory cortex and the high success rate of localization of the visual cortex for participant 001 is bad alignment of the electrodes with the headmodel. As can be seen in Figure 17, the spread of electrodes for participant 001 is far more to the posterior of the head. The participant had a lot of curly hair, which made the alignment of the electrodes with the headmodel problematic. The lack of an individual headmodel could also impact localization.

Localization of multiple functional areas can be performed, but interpretation of the data is complex. The data is retrieved via different processing pipelines, making localization of different functional areas easier. Localization of the somatosensory cortex can still be performed when multiple functional areas are active. The visual cortex is also often active when multiple cortex patches are localized. The localization of the motor cortex is always troublesome.

4.3 The Experiment

Setting up the experiment proved difficult, due to problems with MR PoPe. The previously thought out experiment with multisines would have excited the motor cortex in a different way. Instead of reacting to a twitch motion each time, the participant would have to set the damping and stiffness of the wrist and actively change it based on the frequency content. Hence, MR PoPe should not be used for the application of multisine signals. The haptic robot was intended for use in a MRI scanner, and not with EEG data. A EEG experiment involving a multisine and the identification of the corticomuscular system is not viable, as MR PoPe cannot process these multisine movements.

Better headmodels need to be used during data processing to increase the accuracy of the SL. The currently used headmodels are constructed with the BEM, with source nodes spread throughout the gray and white matter. A standard headmodel was used for the SL of one participant, instead of a unique own headmodel created from a head scan. More detailed headmodels for each participant increase the accuracy of SL.

5 Future Work

First of all, more participants need to be included in the experiment to draw hard conclusions. Two participants, of which one was measured twice, is too shallow of a participant pool to find significant overlap. The potential for human errors to be introduced exists, either by the experimenter or the participant during experimenting. Errors made during these measurements have a significant impact on further conclusions, due to the shallow participant pool.

Several parameters can be improved about the execution of the experiment. These parameters to be improved are presented starting at the end of the data processing and converging back to the beginning of task execution to improve the experiment.

Each participant's own head model should be used during source localization for the most accurate results. It can be used to align the electrodes well onto the headmodel as mentioned in Section 4.3. A better representation of the brain would include the Finite-Element-Method (FEM) method, in which anisotropy can be incorporated in the leadfield [17]. The anisotropy could be acquired by applying a DTI measurement on the participant, which would indicate the neuronal tracts running through the brain.

The source space should only include the pyramidal cells in the grey matter instead of the entire grey and white matter volume. The EEG signal is created by the synchronous activity of neuronal ensembles with the correct orientation [37]. Neighbouring pyramidal cells have the same orientation and can thus create a dipole moment. Neurons in the white matter are oriented random, resulting in a net dipole moment of approximately 0. If only the grey matter was used, the orientation of the dipole moment can be set to be perpendicular to the cortex surface. Currently, the direction of dipoles is optimized during SL, creating dipole orientations probably not in line with anatomy.

Not only the electrodes close to the expected location of activation should be sampled to find significant different areas, as dipoles can project on the electrodes, such that less signal is seen. Multiple electrodes spread over the skin should be sampled to find time (frequency) windows with significant differences.

The current time indices used for ERP SL are determined by ERP level significance testing. However, the source localization per node is already known before significance testing of the EEG data. Hence, it is also possible to perform significance testing on the SL data. The proposed way of significance testing on source data to find meaningful sources cannot be applied to TFR data, as TFR SL relies on the temporal and spectral dimensions selected in the cross-spectral-density matrix constructed to perform TFR SL on.

During preprocessing, the cleaned ERP data was mixed after cleanup using ICA. When independent components are individually inspected, some may have differences that are in line with the task contrasts. For example, the tasks with visual feedback could have an independent component with alpha power attenuation over the entire epoch, while the tasks without visual feedback do not. The mixing of signals impacts theERP and TF window. The current significant windows represent a summation of all neurological processes active in the cerebrum.

Tasks can be added or adjusted. A singular force task without wrist perturbation needs to be added to identify the motor cortex in the absence of activation of the somatosensory cortex by wrist movement. The wrist movement contaminates the data. When the torque task is contrasted with the relax task, the motor cortex cannot be readily identified due to the proximity of the somatosensory cortex. Both can be located using TFR SL in the beta band. Both have power attenuation, only the wrist movement contains power amplification later in the epoch. Adding the task would also complete the factorial design of tasks to be executed by the participant. It would however increase experiment time, and the task would be dull, as no perturbation is active to excite the participant, reducing alertness in the participant.

The visual cortex can be identified using the currently existing model. However, to increase the contrast between activation of the visual cortex, the tasks without visual feedback could be enhanced by placing a blindfold over the participants eyes, excluding any visual inputs. This would increase experimenter/participant interaction and increase experimental time. The participant could also be asked to close their eyes themselves. In this case, a non-visual signal needs to be given to instruct the participant to open their eyes. The current methodology only instructs participants on the upcoming task via text on the visual feedback screen. More pause needs to be given in between tasks to let the paricipant adjust to having their eyes open.

Electrode resistance data needs to be collected before and after the experiment. It shows if the cap came loose or which electrodes gathered worse data over the span of the experiment. These errors can then be accounted for, or the electrode can immediately be deemed a bad channel.

6 Conclusion

The following conclusions can be drawn:

- the somatosensory cortex can correctly and consistently be localized,
- the visual cortex can be localized, but the contrast can be improved by adding an eyes closed task,
- localization of the motor cortex is inconclusive due to the additional presence of wrist movement,
- MR PoPe can be used for transient perturbations,
- individual headmodels need to be created for optimal SL,
- the found localizations need to be compared to a golden standard, such as fMRI,
- the participant pool needs to be enlarged to establish hard conclusions.

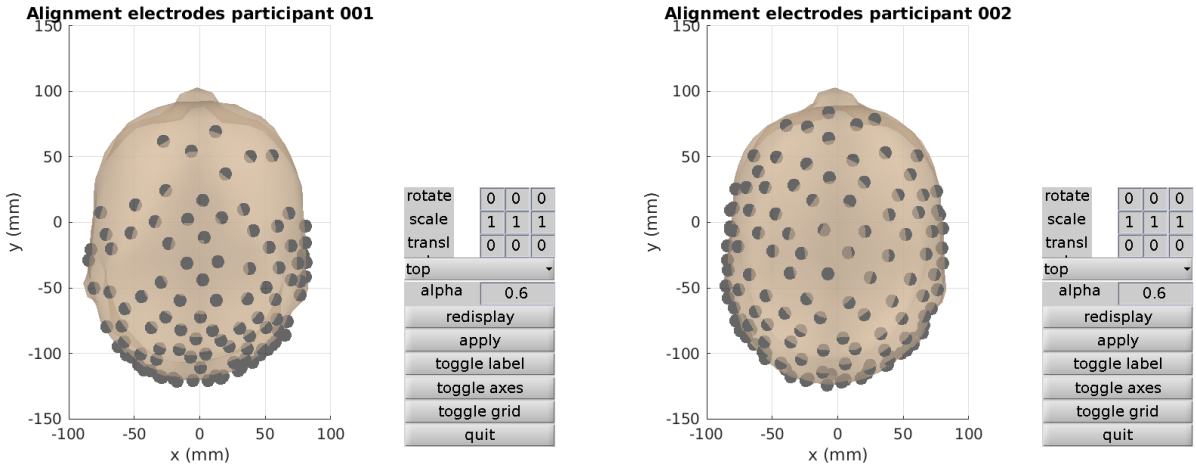

(a) Alignment of the electrodes to the headmodel for participant 001.

(b) Alignment of the electrodes to the headmodel for participant 002 and 022.

Figure 17: A visualization of the alignment of the electrodes to the headmodel after the fiducials are aligned and the electrode locations morphed to the skin. The grey dots indicate an electrode each. As can be seen, the electrodes are aligned more to the posterior for participant 001, compared to 002.

References

[1] G. Abbruzzese, A. Berardelli, J. C. Rothwell, B. L. Day, and C. D. Marsden. Cerebral potentials and electromyographic responses evoked by stretch of wrist muscles in man. *Experimental Brain Research 1985 58:3*, 58(3):544–551, 5 1985. ISSN 1432-1106. doi: 10.1007/BF00235870. URL https://link.springer.com/article/10.1007/BF00235870.

[2] Andrew P. Bagshaw, Eliane Kobayashi, François Dubeau, G. Bruce Pike, and Jean Gotman. Correspondence between EEG-fMRI and EEG dipole localisation of interictal discharges in focal epilepsy. *NeuroImage*, 30(2):417–425, 4 2006. ISSN 10538119. doi: 10.1016/j.neuroimage.2005.09.033.

[3] Dyon Bode, Winfred Mugge, Alfred C. Schouten, Anne Fleur Van Rootselaar, Lo J. Bour, Frans C.T. Van Der Helm, and Piet Lammertse. Design of a magnetic resonance-safe haptic wrist manipulator for movement disorder diagnostics. *Journal of Medical Devices, Transactions of the ASME*, 11(4), 12 2017. ISSN 1932619X. doi: 10.1115/1.4037674/376470. URL https://asmedigitalcollection.asme.org/medicaldevices/article/11/4/045002/376470/Design-of-a-Magnetic-Resonance-Safe-Haptic-Wrist.

[4] Sanne Floor Campfens, Carel G.M. Meskers, Alfred C. Schouten, Michel J.A.M. Van Putten, and Herman Van Der Kooij. Stretch Evoked Potentials in Healthy Subjects and after Stroke: A Potential Measure for Proprioceptive Sensorimotor Function. *IEEE Transactions on Neural Systems and Rehabilitation Engineering*, 23(4):643–654, 7 2015. ISSN 15344320. doi: 10.1109/TNSRE.2015.2388692.

[5] Christoph Christmann, Matthias Ruf, Dieter F. Braus, and Herta Flor. Simultaneous electroencephalography and functional magnetic resonance imaging of primary and secondary somatosensory cortex in humans after electrical stimulation. *Neuroscience Letters*, 333(1):69–73, 11 2002. ISSN 03043940. doi: 10.1016/S0304-3940(02)00969-2. URL https://pubmed.ncbi.nlm.nih.gov/12401562/.

[6] Elisheva R. Coleman, Rohitha Moudgal, Kathryn Lang, Hyacinth I. Hyacinth, Oluwole O. Awosika, Brett M. Kissela, and Wuwei Feng. Early Rehabilitation After Stroke: a Narrative Review. *Current Atherosclerosis Reports*, 19(12), 12 2017. ISSN 15346242. doi: 10.1007/S11883-017-0686-6.

[7] Neva M. Corrigan, Todd Richards, Sara Jane Webb, Michael Murias, Kristen Merkle, Natalia M. Kleinhans, L. Clark Johnson, Andrew Poliakov, Elizabeth Aylward, and Geraldine Dawson. An Investigation of the Relationship Between fMRI and ERP Source Localized Measurements of Brain Activity during Face Processing. *Brain topography*, 22(2):83, 9 2009. ISSN 08960267. doi: 10.1007/S10548-009-0086-5. URL /pmc/articles/PMC4057060//pmc/articles/PMC4057060/?report=abstracthttps://www-ncbi-nlm-nih-gov.tudelft.idm.oclc.org/pmc/articles/PMC4057060/.

[8] B. Neil Cuffin, David Cohen, Kazutomo Yunokuchi, Roman Maniewski, Christopher Purcell, G. Rees Cosgrove, John Ives, John Kennedy, and Donald Schomer. Tests of EEG localization accuracy using implanted sources in the human brain. *Annals of Neurology*, 29(2):132–138, 1991. URL https://sci-hub.se/10.1002/ana.410290204.

[9] Anders M. Dale, Arthur K. Liu, Bruce R. Fischl, Randy L. Buckner, John W. Belliveau, Jeffrey D. Lewine, and Eric Halgren. Dynamic statistical parametric mapping: Combining fMRI and MEG for high-resolution imaging of cortical activity. *Neuron*, 26(1):55–67, 4 2000. ISSN 08966273. doi: 10.1016/S0896-6273(00)81138-1. URL http://www.cell.com/article/S0896627300811381/fulltexthttp://www.cell.com/article/S0896627300811381/abstracthttps://www.cell.com/neuron/abstract/S0896-6273(00)81138-1.

[10] Tom A. de Graaf, Joachim Gross, Gavin Paterson, Tessa Rusch, Alexander T. Sack, and Gregor Thut. Alpha-Band Rhythms in Visual Task Performance: Phase-Locking by Rhythmic Sensory Stimulation. *PLOS ONE*, 8(3):e60035, 3 2013. ISSN 1932-6203. doi: 10.1371/JOURNAL.PONE.0060035. URL https://journals.plos.org/plosone/article?id=10.1371/journal.pone.0060035http://www.nwo.nl/.

[11] Arnaud Delorme and Scott Makeig. EEGLAB: an open source toolbox for analysis of single-trial EEG dynamics including independent component analysis. *Journal of Neuroscience Methods*, 134(1):9–21, 3 2004. ISSN 0165-0270. doi: 10.1016/J.JNEUMETH.2003.10.009.

[12] E. Ray Dorsey, Todd Sherer, Michael S. Okun, and Bastiaan R. Bloemd. The Emerging Evidence of the Parkinson Pandemic. *Journal of Parkinson's disease*, 8(s1):S3–S8, 2018. ISSN 1877-718X. doi: 10.3233/JPD-181474. URL https://pubmed.ncbi.nlm.nih.gov/30584159/.

[13] Elias Ebrahimzadeh, Mohammad Shams, Farahnaz Fayaz, Lila Rajabion, Mahya Mirbagheri, Babak Nadjar Araabi, and Hamid Soltanian-Zadeh. Quantitative determination of concordance in localizing epileptic focus by component-based EEG-fMRI. *Computer methods and programs in biomedicine*, 177:231–241, 8 2019. ISSN 1872-7565. doi: 10.1016/j.cmpb.2019.06.003. URL http://www.ncbi.nlm.nih.gov/pubmed/31319952.

[14] Anteneh M. Feyissa and William O. Tatum. Adult EEG. *Handbook of Clinical Neurology*, 160:103–124, 1 2019. ISSN 0072-9752. doi: 10.1016/B978-0-444-64032-1.00007-2.

[15] Manfred Fuchs, Ralf Drenckhahn, Hans Aloys Wischmann, and Michael Wagner. An improved boundary element method for realistic volume-conductor modeling. *IEEE Transactions on Biomedical Engineering*, 45(8):980–997, 8 1998. ISSN 00189294. doi: 10.1109/10.704867.

[16] J. Gross, J. Kujala, M. Hämäläinen, L. Timmermann, A. Schnitzler, and R. Salmelin. Dynamic imaging of coherent sources: Studying neural interactions in the human brain. *Proceedings of the National Academy of Sciences of the United States of America*, 98(2):694–699, 1 2001. ISSN 00278424. doi: 10.1073/PNAS.98.2.694. URL www.pnas.org.

[17] Daniel Güllmar, Jens Haueisen, and Jürgen R. Reichenbach. Influence of anisotropic electrical conductivity in white matter tissue on the EEG/MEG forward and inverse solution. A high-resolution whole head simulation study. *NeuroImage*, 51(1):145–163, 5 2010. ISSN 10538119. doi: 10.1016/j.neuroimage.2010.02.014.

[18] M. S. Hämäläinen and R. J. Ilmoniemi. Interpreting magnetic fields of the brain: minimum norm estimates. *Medical & Biological Engineering & Computing*, 32(1):35–42, 1 1994. ISSN 0140-0118. doi: 10.1007/BF02512476. URL http://link.springer.com/10.1007/BF02512476.

[19] Stefan Haufe, Paul DeGuzman, Simon Henin, Michael Arcaro, Christopher J. Honey, Uri Hasson, and Lucas C. Parra. Elucidating relations between fMRI, ECoG, and EEG through a common natural stimulus. *NeuroImage*, 179:79–91, 10 2018. ISSN 10959572. doi: 10.1016/j.neuroimage.2018.06.016.

[20] David J. Heeger, Alex C. Huk, Wilson S. Geisler, and Duane G. Albrecht. Spikes versus BOLD: What does neuroimaging tell us about neuronal activity? *Nature Neuroscience*, 3(7):631–633, 7 2000. ISSN 10976256. doi: 10.1038/76572.

[21] Chang Hwan Im, Arvind Gururajan, Nanyin Zhang, Wei Chen, and Bin He. Spatial resolution of EEG cortical source imaging revealed by localization of retinotopic organization in human primary visual cortex. *Journal of Neuroscience Methods*, 161(1):142–154, 3 2007. ISSN 01650270. doi: 10.1016/j.jneumeth.2006.10.008.

[22] Silke Klamer, Adham Elshahabi, Holger Lerche, Christoph Braun, Michael Erb, Klaus Scheffler, and Niels K Focke. Differences between MEG and high-density EEG source localizations using a distributed source model in comparison to fMRI. *Brain topography*, 28(1):87–94, 1 2015. ISSN 1573-6792. doi: 10.1007/s10548-014-0405-3. URL http://www.ncbi.nlm.nih.gov/pubmed/25296614.

[23] Ching-Chang Kuo, Phan Luu, Kyle K. Morgan, Mark Dow, Colin Davey, Jasmine Song, Allen D. Malony, and Don M. Tucker. Localizing Movement-Related Primary Sensorimotor Cortices with Multi-Band EEG Frequency Changes and Functional MRI. *PLoS ONE*, 9(11):e112103, 11 2014. ISSN 1932-6203. doi: 10.1371/journal.pone.0112103. URL https://dx.plos.org/10.1371/journal.pone.0112103.

[24] A M Lascano, F Grouiller, M Genetti, L Spinelli, M Seeck, K Schaller, and C M Michel. Surgically Relevant Localization of the Central Sulcus With High-density SEP Compared to fMRI. *Neurosurgery*, 2014. doi: 10.1227/NEU.0000000000000298. URL http://www.ncbi.nlm.nih.gov/pubmed/24463494.

[25] Louis Lemieux, Karsten Krakow, and David R. Fish. Comparison of spike-triggered functional MRI BOLD activation and EEG dipole model localization. *NeuroImage*, 14(5):1097–1104, 11 2001. ISSN 10538119. doi: 10.1006/nimg.2001.0896. URL http://www.ncbi.nlm.nih.gov/pubmed/11697941.

[26] Fa Hsuan Lin, Thomas Witzel, Matti S. Hämäläinen, Anders M. Dale, John W. Belliveau, and Steven M. Stufflebeam. Spectral spatiotemporal imaging of cortical oscillations and interactions in the human brain. *NeuroImage*, 23(2):582–595, 10 2004. ISSN 1053-8119. doi: 10.1016/J.NEUROIMAGE.2004.04.027.

[27] Quanying Liu, Marco Ganzetti, Nicole Wenderoth, and Dante Mantini. Detecting large-scale brain networks using EEG: Impact of electrode density, head modeling and source localization. *Frontiers in Neuroinformatics*, 12, 3 2018. ISSN 16625196. doi: 10.3389/fninf.2018.00004.

[28] Nikos K. Logothetis. What we can do and what we cannot do with fMRI. *Nature*, 453(7197):869–878, 6 2008. ISSN 14764687. doi: 10.1038/NATURE06976.

[29] Nikos K. Logothetis and Brian A. Wandell. Interpreting the BOLD Signal. *Annual Review of Physiology*, 66(1):735–769, 3 2004. ISSN 0066-4278. doi: 10.1146/annurev.physiol.66.082602.092845.

[30] Nikos K. Logothetis, Hellmut Merkle, Mark Augath, Torsten Trinath, and Kâmil Uğurbil. Ultra High-Resolution fMRI in Monkeys with Implanted RF Coils. *Neuron*, 35(2):227–242, 7 2002. ISSN 0896-6273. doi: 10.1016/S0896-6273(02)00775-4.

[31] E.N. Marieb and K. Hoehn. *Human Anatomy & Physiology*. Pearson Education Limited, Harlow, 10 edition, 2015.

[32] Eric Maris and Robert Oostenveld. Nonparametric statistical testing of EEG- and MEG-data. *Journal of Neuroscience Methods*, 164(1):177–190, 8 2007. ISSN 0165-0270. doi: 10.1016/J.JNEUMETH.2007.03.024.

[33] Yaron Meirovitch, Hila Harris, Eran Dayan, Amos Arieli, and Tamar Flash. Alpha and Beta Band Event-Related Desynchronization Reflects Kinematic Regularities. *Journal of Neuroscience*, 35(4):1627–1637, 1 2015. ISSN 0270-6474. doi: 10.1523/JNEUROSCI.5371-13.2015. URL https://www.jneurosci.org/content/35/4/1627https://www.jneurosci.org/content/35/4/1627.abstract.

[34] Winfred Mugge, David A. Abbink, and Frans C.T. Van Der Helm. Reduced power method: How to evoke low-bandwidth behaviour while estimating full-bandwidth dynamics. In *2007 IEEE 10th International Conference on Rehabilitation Robotics, ICORR'07*, pages 575–581, 2007. ISBN 1424413206. doi: 10.1109/ICORR.2007.4428483.

[35] Christoph Mulert, Lorenz Jäger, Robert Schmitt, Patrick Bussfeld, Oliver Pogarell, Hans Jürgen Möller, Georg Juckel, and Ulrich Hegerl. Integration of fMRI and simultaneous EEG: Towards a comprehensive understanding of localization and time-course of brain activity in target detection. *NeuroImage*, 22(1):83–94, 5 2004. ISSN 10538119. doi: 10.1016/j.neuroimage.2003.10.051.

[36] R. C. Oldfield. The assessment and analysis of handedness: The Edinburgh inventory. *Neuropsychologia*, 9(1):97–113, 3 1971. ISSN 0028-3932. doi: 10.1016/0028-3932(71)90067-4.

[37] Piotr Olejniczak. Neurophysiologic Basis of EEG. *Journal of Clinical Neurophysiology*, 23(3):186–189, 6 2006. ISSN 0736-0258. doi: 10.1097/01.wnp.0000220079.61973.6c. URL http://journals.lww.com/00004691-200606000-00002.

[38] Robert Oostenveld, Pascal Fries, Eric Maris, and Jan-Mathijs Schoffelen. FieldTrip: Open Source Software for Advanced Analysis of MEG, EEG, and Invasive Electrophysiological Data. *Computational Intelligence and Neuroscience*, 2011, 2011. doi: 10.1155/2011/156869. URL http://www.mathworks.com.

[39] R. D. Pascual-Marqui, Christoph M. Michel, and Dietrich Lehmann. Low Resolution Electromagnetic Tomography: A New Method for Localizing Electrical Activity in the Brain., 1994. URL https://www.uzh.ch/keyinst/NewLORETA/BriefHistory/LORETA-paper02.pdf.

[40] Ioannis Petridis. Nonlinearity in the Light Processing of the Human Visual System. Technical report, Delft University of Technology, Delft, 6 2017.

[41] Rik Pintelon and Johan Schoukens. *System Identification: A Frequency Domain Approach*. John Wiley & Sons, Inc., Hoboken, 2nd edition, 2012. ISBN 9780470640371.

[42] Sabrina Pitzalis, Francesca Strappini, Marco De Gasperis, Alessandro Bultrini, and Francesco Di Russo. Spatio-Temporal Brain Mapping of Motion-Onset VEPs Combined with fMRI and Retinotopic Maps. *PLoS ONE*, 7(4):e35771, 4 2012. ISSN 1932-6203. doi: 10.1371/journal.pone.0035771. URL http://dx.plos.org/10.1371/journal.pone.0035771.

[43] Masa Aki Sato, Taku Yoshioka, Shigeki Kajihara, Keisuke Toyama, Naokazu Goda, Kenji Doya, and Mitsuo Kawato. Hierarchical Bayesian estimation for MEG inverse problem. *NeuroImage*, 23(3):806–826, 11 2004. ISSN 1053-8119. doi: 10.1016/J.NEUROIMAGE.2004.06.037.

[44] Alexander J. Shackman, Brenton W. McMenamin, Heleen A. Slagter, Jeffrey S. Maxwell, Lawrence L. Greischar, and Richard J. Davidson. Electromyogenic artifacts and electroencephalographic inferences, 6 2009. ISSN 08960267. URL /pmc/articles/PMC2712576/?report=abstracthttps://www.ncbi.nlm.nih.gov/pmc/articles/PMC2712576/.

[45] S. Sharifi, F. Luft, L. de Boer, A. W.G. Buijink, W. Mugge, A. C. Schouten, T. Heida, L. J. Bour, and A. F. van Rootselaar. Closing the loop: Novel quantitative fMRI approach for manipulation of the sensorimotor loop in tremor. *NeuroImage*, 262:119554, 11 2022. ISSN 1053-8119. doi: 10.1016/J.NEUROIMAGE.2022.119554.

[46] Dahlia Sharon, Matti S. Hämäläinen, Roger B.H. Tootell, Eric Halgren, and John W. Belliveau. The advantage of combining MEG and EEG: Comparison to fMRI in focally stimulated visual cortex. *NeuroImage*, 36(4):1225–1235, 7 2007. ISSN 10538119. doi: 10.1016/j.neuroimage.2007.03.066.

[47] Stephen D. Silberstein. Migraine. *The Lancet*, 363(9406):381–391, 1 2004. ISSN 0140-6736. doi: 10.1016/S0140-6736(04)15440-8. URL http://www.thelancet.com/article/S0140673604154408/fulltexthttp://www.thelancet.com/article/S0140673604154408/abstracthttps://www.thelancet.com/journals/lancet/article/PIIS0140-6736(04)15440-8/abstract.

[48] Melissa M. Smith, Kurt E. Weaver, Thomas J. Grabowski, Rajesh P.N. Rao, and Felix Darvas. Non-invasive detection of high gamma band activity during motor imagery. *Frontiers in Human Neuroscience*, 8(OCT), 10 2014. ISSN 16625161. doi: 10.3389/fnhum.2014.00817.

[49] Catherine Tallon-Baudry and Olivier Bertrand. Oscillatory gamma activity in humans and its role in object representation. *Trends in Cognitive Sciences*, 3(4):151–162, 4 1999. ISSN 13646613. doi: 10.1016/S1364-6613(99)01299-1. URL http://www.cell.com/article/S1364661399012991/fulltexthttp://www.cell.com/article/S1364661399012991/abstracthttps://www.cell.com/trends/cognitive-sciences/abstract/S1364-6613(99)01299-1.

[50] S Thees, F Blankenburg, B Taskin, G Curio, and A Villringer. Dipole source localization and fMRI of simultaneously recorded data applied to somatosensory categorization. 2003. doi: 10.1016/S1053-8119(02)00054-X. URL www.elsevier.com/locate/ynimg.

[51] Deborah Vitacco, Daniel Brandeis, Roberto Pascual-Marqui, and Ernst Martin. Correspondence of event-related potential tomography and functional magnetic resonance imaging during language processing. *Human Brain Mapping*, 17(1):4–12, 9 2002. ISSN 10659471. doi: 10.1002/hbm.10038. URL https://pubmed.ncbi.nlm.nih.gov/12203683/.

[52] Martijn P. Vlaar, Winfred Mugge, Paul F.C. Groot, Sarvi Sharifi, Lo J. Bour, Frans C.T. van der Helm, Anne Fleur van Rootselaar, and Alfred C. Schouten. Targeted brain activation using an MR-compatible wrist torque measurement device and isometric motor tasks during functional magnetic resonance imaging. *Magnetic Resonance Imaging*, 34(6):795–802, 7 2016. ISSN 18735894. doi: 10.1016/J.MRI.2016.02.002.

[53] S. Vulliemoz, R. Thornton, R. Rodionov, D.W. Carmichael, M. Guye, S. Lhatoo, A.W. McEvoy, L. Spinelli, C. M. Michel, J. S. Duncan, L. Lemieux, S Vulliemoz, R Thornton, R Rodionov, D W Carmichael, M Guye, S Lhatoo, A W McEvoy, L Spinelli, C M Michel, J S Duncan, and L Lemieux. The spatio-temporal mapping of epileptic networks: combination of EEG-fMRI and EEG source imaging. *NeuroImage*, 46(1095-9572 (Electronic)):834–843, 7 2009. ISSN 1053-8119. URL http://www.embase.com/search/results?subaction=viewrecord&from=export&id=L50447427http://dx.doi.org/10.1016/j.neuroimage.2009.01.070http://sfx.library.uu.nl/utrecht?sid=EMBASE&issn=10538119&id=doi:10.1016/j.neuroimage.2009.01.070&atitle=The+spatio-tem.

[54] Jun Yao and Julius P.A. Dewald. Evaluation of different cortical source localization methods using simulated and experimental EEG data. *NeuroImage*, 25(2):369–382, 4 2005. ISSN 10538119. doi: 10.1016/j.neuroimage.2004.11.036. URL https://linkinghub.elsevier.com/retrieve/pii/S1053811904007219.

[55] Han Yuan, Tao Liu, Rebecca Szarkowski, Cristina Rios, James Ashe, and Bin He. Negative covariation between task-related responses in alpha/beta-band activity and BOLD in human sensorimotor cortex: An EEG and fMRI study of motor imagery and movements. *NeuroImage*, 49(3):2596–2606, 2 2010. ISSN 10538119. doi: 10.1016/j.neuroimage.2009.10.028. URL https://linkinghub.elsevier.com/retrieve/pii/S1053811909010994.

Appendices

A Schematics of EEG Data Acquisition

The schematic overview of the EEG data acquisition is shown in Figure 18. The setup consists of a laptop, MR PoPe and the accompanying manipulandum, a 128 electrode EEG cap with accompanying ReFa amplifier and usb-converter (tMSI, Netherlands), EMG sensors and a computer screen. The perturbation to be presented is uploaded to MR PoPe before the start of the experiment. During the experiment, the mechanical perturbation is send from MR PoPe to the MR PoPe manipulandum. The manipulandum sends back information about the torque (Tor) and position (Pos) applied to the manipulandum and therefore the wrist to MR PoPe. The mechanical perturbation is processed by the participant CNS. From the participant, EMG and EEG data is transferred to the ReFa amplifier (tMSI, Netherlands). MR PoPe also sends the postion, torque and trigger data to the ReFa amplifier. The data is synchronized at the amplifier as the measurements enter at the same time and continuously. The ReFa sends all information via a usb converter to the laptop. The laptop filters the necessary input data for the task and supplies it to the feedback screen, where it is shown to the participant.

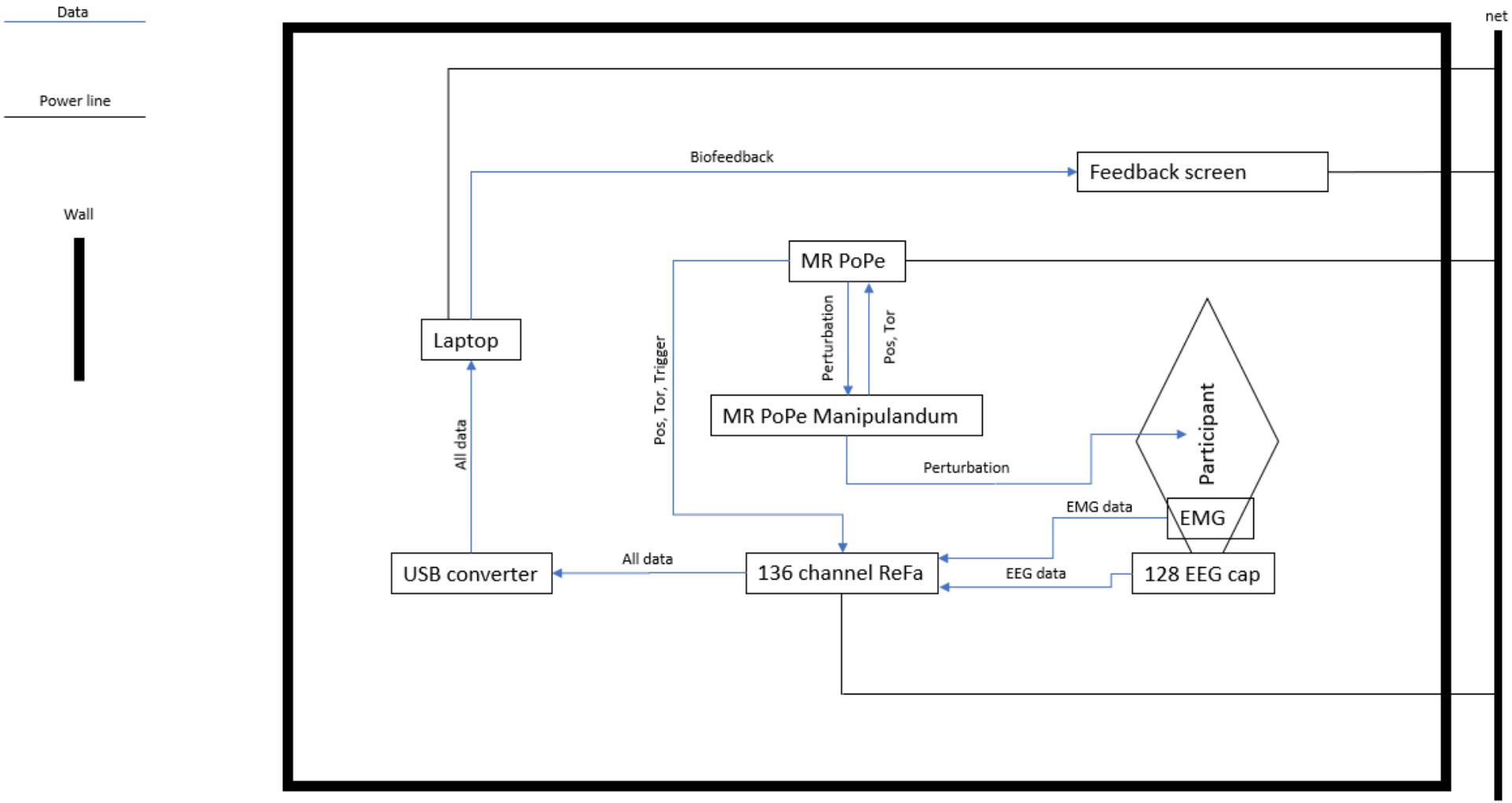

Figure 18: The schematic overview of EEG data acquisition. The setup consists of a laptop, MR PoPe and the accompanying manipulandum, a 128 electrode EEG cap with accompanying ReFa amplifier and usb-converter (tMSI, Netherlands), EMG sensors and a computer screen. The perturbation to be presented is uploaded to MR PoPe before the start of the experiment. During the experiment, the mechanical perturbation is send from MR PoPe to the MR PoPe manipulandum. The manipulandum sends back information about the torque (Tor) and position (Pos) data applied to the manipulandum and therefore the wrist. The perturbation is processed by the CNS of the participant. From the participant, EMG and EEG data is transferred to the ReFa amplifier (tMSI, Netherlands). MR PoPe also sends the postion, torque and trigger data to the ReFa amplifier. The ReFa sends all information via a usb converter to the laptop. The laptop filters the necessary input data for the task and supplies it to the feedback screen, where it is shown to the participant.